The structure of the Myo4p globular tail and its function in ASH1 mRNA localization

Alexander Heuck,^{1,2} Ingrid Fetka,³ Daniel N. Brewer,⁴ Daniela Hüls,^{1,2} Mary Munson,⁴ Ralf-Peter Jansen,³ and Dierk Niessing^{1,2,5}

¹Institute of Structural Biology, Helmholtz Zentrum München, German Research Center for Environmental Health, 81377 Munich, Germany

ype V myosin (MyoV)-dependent transport of cargo is an essential process in eukaryotes. Studies on yeast and vertebrate MyoV showed that their globular tails mediate binding to the cargo complexes. In Saccharomyces cerevisiae, the MyoV motor Myo4p interacts with She3p to localize asymmetric synthesis of HO 1 (ASH1) mRNA into the bud of dividing cells. A recent study showed that localization of GFP-MS2-tethered ASH1 particles does not require the Myo4p globular tail, challenging the supposed role of this domain. We assessed ASH1 mRNA and Myo4p distribution more directly

and found that their localization is impaired in cells expressing globular tail–lacking Myo4p. In vitro studies further show that the globular tail together with a more N-terminal linker region is required for efficient She3p binding. We also determined the x-ray structure of the Myo4p globular tail and identify a conserved surface patch important for She3p binding. The structure shows pronounced similarities to membrane-tethering complexes and indicates that Myo4p may not undergo auto-inhibition of its motor domain.

Introduction

Type V myosins are highly conserved motor proteins that transport organelles, vesicles, proteins, and mRNAs (Vale, 2003). They consist of an N-terminal motor domain, followed by a regulatory lever arm and a tail region. The tail contains a coiled-coil region, followed by a short linker and a C-terminal globular tail domain (Fig. 1 A; Reck-Peterson et al., 2000). Previous studies suggested that the main function of the globular tail domain is cargo binding (Vale, 2003). A recent study in yeast, however, showed that GFP-MS2-tethered messenger ribonucleoprotein particles (mRNPs) are efficiently transported by a globular tail-lacking mutant of the type V myosin Myo4p (Bookwalter et al., 2009).

Myo4p translocates *ASH1* mRNA plus more than 30 other mRNAs as well as ER into the bud (Müller et al., 2007; Paquin and Chartrand, 2008). This bud-tip localization of *ASH1* mRNA and the subsequent bud-localized translation of Ash1p prevents

Correspondence to Dierk Niessing: niessing@helmholtz-muenchen.de

Abbreviations used in this paper: ASH, asymmetric synthesis of HO; COG, conserved oligomeric Golgi; GT, globular tail; MyoV, type V myosin; RMSD, root-mean-square deviation; She, Swi5p-dependent HO expression; She3p-N, N-terminal half of She3p.

mating-type switching exclusively in the bud (Bobola et al., 1996; Jansen et al., 1996). *ASH1* mRNA localization is a multistep process that involves (i) nuclear mRNP formation, (ii) assembly of the cytoplasmic transport complex and translational silencing, (iii) Myo4p-dependent mRNP transport to the bud tip, (iv) anchoring at the bud tip and remodeling of the mRNP, and eventually (v) translational activation of *ASH1* mRNA after cytokinesis.

Besides Myo4p itself, mRNA localization depends on its binding partner She3p and the She3p-associated RNA-binding protein She2p (Müller et al., 2007; Paquin and Chartrand, 2008). Inheritance of cortical ER is independent of She2p and mRNA but still requires the myosin motor and the adapter protein She3p (Estrada et al., 2003). Thus, Myo4p interaction with She3p is required for the localization of both cargoes. For this interaction, the N-terminal half of She3p (She3p-N; aa 1–234)

© 2010 Heuck et al. This article is distributed under the terms of an Attribution–Noncommercial–Share Alike–No Mirror Sites license for the first six months after the publication date (see http://www.rupress.org/terms). After six months it is available under a Creative Commons License (Attribution–Noncommercial–Share Alike 3.0 Unported license, as described at http://creativecommons.org/licenses/by-nc-sa/3.0/).

Supplemental Material can be found at: http://jcb.rupress.org/content/suppl/2010/04/30/jcb.201002076.DC1.html Downloaded from jcb.rupress.org on May 4, 2010

²Gene Center and Department of Biochemistry, Ludwig-Maximilians-University Munich, 81377 Munich, Germany

³University of Tübingen, Interfaculty Institute for Biochemistry, 72076 Tübingen, Germany

⁴Department of Biochemistry and Molecular Pharmacology, University of Massachusetts Medical School, Worcester, MA 01605

⁵Munich Center for Integrated Protein Science, 81377 Munich, Germany

binds to two independent regions of the Myo4p tail (Böhl et al., 2000; Estrada et al., 2003; Heuck et al., 2007). The more N-terminal region contains the coiled-coil domain (aa 923–1042; Fig. 1 A). The C-terminally located She3p-binding region (aa 1042–1471) includes the short linker region and a putative globular tail. Because the globular tail has been reported to be dispensable for in vivo transport of GFP-MS2–tethered reporter mRNAs (Bookwalter et al., 2009), it was suggested that She3p binding is restricted to regions N-terminal of the globular tail. The report further implied that the globular tail might lack functional importance.

In this study we confirmed the correct localization of ER or GFP-MS2–tethered particles upon deletion of the Myo4p globular tail. However, we also found that deletion of the globular tail resulted in impaired She3p binding in vitro. This finding seemed to contradict the previous suggestion that the globular tail might be dispensable for Myo4p-dependent mRNA transport (Bookwalter et al., 2009). We therefore reassessed the potential role of the globular tail of Myo4p in vivo, in vitro, and by x-ray crystallography. Inspection of cells expressing globular tail—lacking Myo4p yielded that mating type switching, as well as Myo4p and *ASH1* mRNA localization, is impaired. These findings indicate that GFP-MS2–tethered particles do not always faithfully recapitulate the endogenous localization of mRNAs.

x-ray structure determination of the Myo4p globular tail yielded significant conservation to the only published structure of a MyoV globular tail (from Myo2p; Pashkova et al., 2006) and to components of three distinct membrane-tethering complexes. Moreover, residues known from other type V myosins to be important for motor auto-inhibition are lacking in the respective positions on the Myo4p structure. It suggests that Myo4p does not undergo globular tail–dependent auto-inhibition in the previously described fashion.

Results

Defining the domain boundaries of the Myo4p globular tail

For a comprehensive analysis of She3p binding to the Myo4p tail, we first identified the boundaries of the globular part of the Myo4p tail by limited proteolysis. After Glu-C protease digestion, we observed a protease-resistant fragment of \sim 45 kD (Fig. S1 A) starting at aa 1091 (Fig. 1 A), as identified by Edman sequencing. The experimentally determined approximate boundaries of the globular tail indicate that the Myo4p tail (aa 923–1471) is subdivided into the coiled coil–containing region (aa 923–1041), the globular tail (aa 1091–1471; GT), and a protease-sensitive linker (aa 1042–1090; L) (Fig. 1 A).

Recent domain-swapping and -deletion experiments showed that C-terminally truncated Myo4p with a stop codon after aa 1068 efficiently localizes large GFP-MS2-tethered ASH1 mRNA particles as well as ER (Bookwalter et al., 2009). According to our experimental domain mapping, this deletion includes the globular tail plus more than 20 residues of the protease-sensitive linker region. We were interested if a Myo4p fragment with a deletion of the experimentally

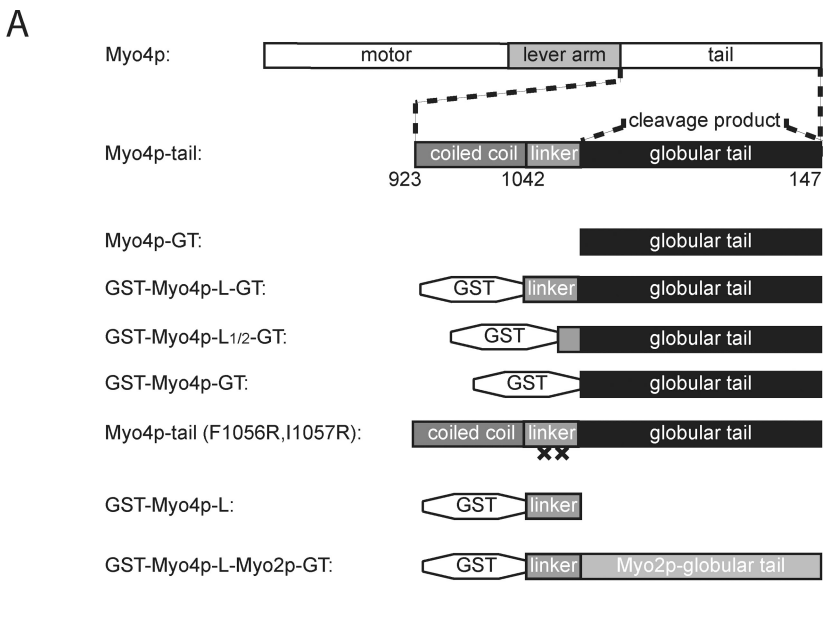
refined globular tail shows a comparable behavior. We therefore analyzed the localization of GFP-MS2-tethered *ASH1* particles and of ER in response to a Myo4p motor with a stop codon after residue 1090. This truncated motor also localizes GFP-MS2 particles and inherits ER in a manner undistinguishable from full-length Myo4p (Fig. S1, B–F). Thus, our results confirm the previous findings of Bookwalter et al. (2009).

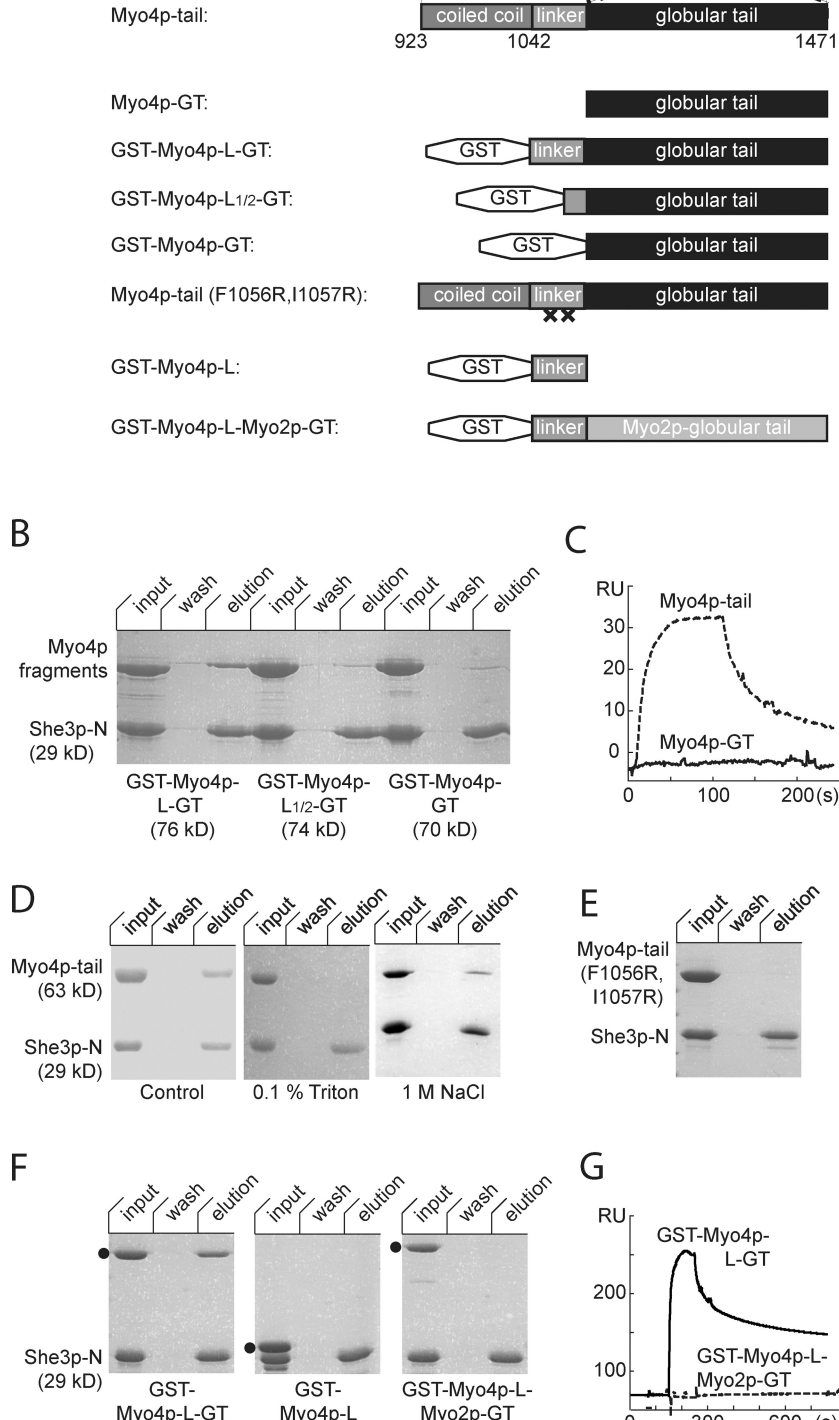
The linker in the Myo4p tail is required for efficient She3p binding

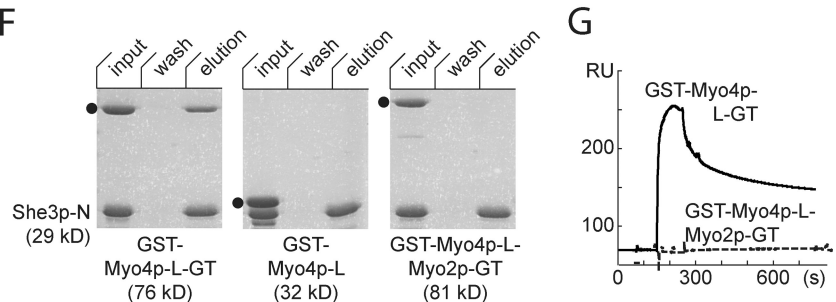
These results suggested that the globular tail might also be dispensable for She3p binding. To directly map the She3p-binding region of Myo4p, we immobilized His-tagged She3p-N on Ni-sepharose beads and performed pull-down experiments with different GST-tagged Myo4p fragments. These fragments contained the globular tail and linker regions of decreasing length, starting from residue 1042 (GST-Myo4p-L-GT), 1063 (GST-Myo4p-L_{1/2}-GT), or 1091 (GST-Myo4p-GT), respectively (Fig. 1 A). The N-terminal fusion of GST ensured dimerization-dependent complex stabilization known to be required for pull-down reactions (Heuck et al., 2007). Previous binding studies with GST-Myo4p-L-GT and She3p using surface plasmon resonance (SPR) showed that they interact with an equilibrium-dissociation constant (Kd) of 330 nM (Heuck et al., 2007). As expected, an interaction was observed with She3p-N and the GST-Myo4p-L-GT fragment (Fig. 1 B). In contrast, no significant binding was observed between She3p-N and the GST-Myo4p- $L_{1/2}$ -GT or the GST-Myo4p-GT fragment (Fig. 1 B). Thus, the protease-sensitive linker region in the tail seems important for full She3p binding.

Pull-down experiments often fail to detect weak and/or transient interactions. We therefore tested binding of the Myo4p globular tail fragment by SPR. Also with this method, we detected no interaction of the globular tail with She3p-N, even at $5 \mu M$ concentration (Fig. 1 C).

Sequence analysis of the linker predicted a hydrophobic region between amino acids 1055 and 1060 (Fig. S1 G). Hydrophobic sequence stretches have a high probability to be involved in intra- or intermolecular protein interactions (Tsai et al., 1997). Because the linker is highly protease sensitive (Fig. S1 A) and thus might lack a globular fold, we speculated that its hydrophobic amino acids might rather be involved in protein-protein interactions than in local folding events. To test such a hydrophobic contribution in She3p binding, we performed pull-down experiments with She3p-N and the entire Myo4p tail in the presence or absence of a detergent. For this interaction without detergent, a Kd of 172 nM had previously been measured (Heuck et al., 2007). As expected, a strong interaction was observed in the previously used buffer conditions (Fig. 1 D, left; Heuck et al., 2007). However, the addition of 0.1% Triton X-100 completely abolished this interaction (Fig. 1 D, middle). Increasing the ionic strength of a buffer stabilizes hydrophobic interactions, whereas interactions involving charged amino acids are weakened. Pull-down experiments in buffer containing 1 M NaCl still resulted in a considerable binding (Fig. 1 D, right), suggesting a hydrophobic







contribution to the interaction. To find out whether these findings are linked to the hydrophobic patch in the linker, we exchanged the hydrophobic residues phenylalanine in position 1056 and isoleucine in position 1057 in the linker region with arginines (Myo4p-tail (F1056R, I1057R); Fig. 1 A). Correct overall folding and solubility of this mutant protein was

confirmed by size-exclusion chromatography (not depicted). In pull-down experiments, Myo4p-tail (F1056R, I1057R) failed to interact with She3p-N (Fig. 1 E; positive control in Fig. 1 D, left). In summary, these results indicate that hydrophobic residues within the linker region of the Myo4p tail contribute to She3p binding.

Figure 1. Efficient She3p binding to Myo4p requires the protease-sensitive linker and the globular tail. (A) Cartoon representation of Myo4p fragments. The full Myo4p tail consists of a coiled-coil region, a linker region, and a sequence stretch with 25% homology to the globular tail of Myo2p. Limited proteolysis experiments with the Myo4p tail fragment revealed a stable cleavage product of 45 kD (Fig. S1 A), which was identified as the globular tail. (B) Ni-sepharose pull-down reactions with immobilized His-She3p-N and different Myo4p constructs indicate that the protease-sensitive linker is required for efficient She3p-N binding. (C) Surface-plasmon resonance (SPR) with surface-coupled She3p-N reveals efficient binding of the Myo4p tail, whereas no binding was observed for the globular tail at concentrations up to 5 µM. (D) Pull-down reactions as in B with Myo4p tail in standard buffer (left), buffer containing additional 0.1% Triton X-100 (middle), or buffer containing 1 M NaCl (right). (E) Pull-down reaction as in D with a mutated Myo4p tail fragment (Myo4p-tail (F1056R, I1057R); see A). This fragment failed to reveal binding under standard conditions. (F) Pull-down reactions as in B with GST-Myo4p-L-GT (left), with a globular tail-lacking Myo4p fragment (GST-Myo4p-L; middle), or with a Myo4p fragment that has exchanged its globular tail with the corresponding domain of its paralogue Myo2p (GST-Myo4p-L-Myo2p-GT; right). Dots indicate the position of the respective Myo4p fragments. Note that in the input lane of the middle image, the top band is Myo4p, the middle band is She3p, and the bottom band is a degradation product of Myo4p. (G) SPR with surface-coupled She3p-N reveals efficient binding of the GST-Myo4p-L-GT, whereas no binding was observed even at $\sim 10~\mu M$ when the globular tail was exchanged for the corresponding domain of Myo2p (GST-Myo4p-L-Myo2p-GT).

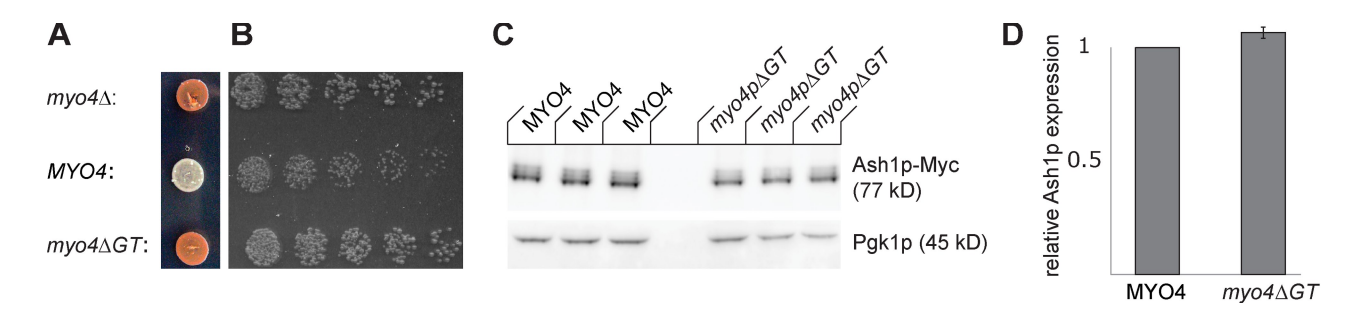


Figure 2. Asymmetric distribution of Ash1 protein. (A) A white/red assay was used to assess localized ASH1-mRNA translation. White color indicates correct asymmetric distribution of Ash1p, whereas a red color indicates defects in this process. As expected, Myo4p knock-out cells show a red color when grown on adenine-deficient media whereas wild-type Myo4p-expressing cells are white. $myo4\Delta GT$ cells show a red color. (B) On media containing 0.03% canavanine, $myo4\Delta$ and $myo4\Delta$ GT cells grow identically, whereas MYO4 cells show an impaired growth. Both experiments suggest the requirement of the globular tail domain for localized ASH1-mRNA translation at the tip of the daughter cell. (C and D) Assessment of Ash1p expression levels in wild-type and myo4AGT cells by quantitative Western blot. (C) Exemplary Western blot with each sample loaded three times for accurate quantification of Ash1p-Myc and Pgk1p expression levels. (D) The relative expression of Ash1p showed no considerable difference between wild-type and myo4\DGT cells. We normalized the expression of Ash1p relatively to Pgk1p by setting their ratio to one in Myo4p wild-type cells. Three independent experiments were performed for each strain.

The Myo4p globular tail is required for efficient She3p binding

To test whether the linker is sufficient for stable complex formation with She3p, we performed pull-down assays with She3p-N and a globular tail-lacking Myo4p fragment (GST-Myo4p-L; Fig. 1 A). The GST-Myo4p-L fragment could not be pulled down by She3p-N (Fig. 1 F, middle). However, because we also observed a weak tendency of GST-Myo4p-L to degrade (see degradation band at bottom of Fig. 1 F, middle) the lack of binding could either mean that the globular tail is required for She3p binding or that it is simply a result of linker degradation.

To assess the latter possibility, we generated a hybrid fragment in which we fused GST-Myo4p-L with the globular tail of the paralogue Myo2p (GST-Myo4p-L-Myo2p-GT; Fig. 1 A). As expected, the globular tail of Myo2p protected the GST-Myo4p-L fragment from degradation (see input lane in Fig. 1 F, right). In pull-down experiments, however, GST-Myo4p-L-Myo2p-GT yielded no binding to She3p-N (Fig. 1 F, right). To detect potential transient interactions that might have escaped detection in pull-down assays, we also tested GST-Myo4p-L-Myo2p-GT in SPR experiments. These SPR experiments failed to show an interaction with immobilized She3p-N, even at a protein concentration of $\sim 10 \, \mu M$ (Fig. 1 G). In contrast, the GST-tagged Myo4p fragment consisting of the linker and the endogenous globular tail (GST-Myo4p-L-GT) binds She3p-N with a Kd of 330 nM (Heuck et al., 2007) and interacted efficiently with She3p-N in our current experiments (Fig. 1, B, F, and G). Together, these results indicate that the linker and the globular tail domain provide a composite binding region for She3p.

Deletion of the Myo4p globular tail results in impaired mother cell-specific expression of HO endonuclease

The Myo4p globular tail is not required for the localization of GFP-MS2-tethered ASH1 particles (Fig. S1, D-F; Bookwalter et al., 2009). Our in vitro binding studies, however, point toward a functional requirement of the globular tail for full She3p binding (Fig. 1, F and G). Because GFP-MS2-tethered

reporter particles show clear differences to endogenous particles (Bertrand et al., 1998; Lange et al., 2008) and because these previous analyses did not include an assessment of correct translation upon localization, we wondered if potential defects could have remained undetected by the GFP-MS2 reporter approach.

We therefore tested the importance of the Myo4p globular tail for the in vivo function of ASH1-mRNA localization, i.e., the mother cell-specific expression of HO endonuclease. We used a previously established assay (Jansen et al., 1996) in which the promoters of CAN1 and ADE2 were replaced with that from the HO endonuclease. Cells with such exchanged promoters accumulate a red-colored pigment under adeninedeficient conditions and become resistant to canavanine whenever the correct localized translation of ASH1 mRNA fails. As expected, colonies from the $myo4\Delta$ strain appeared red when grown on plates with reduced adenine levels (Fig. 2 A), indicating impaired daughter cell-specific Ash1p accumulation. In contrast, wild-type Myo4p-expressing colonies (MYO4) showed a white color (Fig. 2 A). Like $myo4\Delta$, the $myo4\Delta GT$ strain showed a red coloration, indicating a requirement of the globular tail for localized ASH1-mRNA translation (Fig. 2 A). To assess the defect of localized ASH1-mRNA translation by canavanine sensitivity, we compared the growth of yeast colonies from these strains on canavanine-containing media. This experiment revealed no detectable difference between the $myo4\Delta$ and $myo4\Delta GT$ strains, whereas the growth of MYO4 cells was reduced (Fig. 2 B). Thus, the globular tail of Myo4p is not only involved in the She3p interaction in vitro (Fig. 1, F and G), but also required for correct control of HO expression in vivo.

Ash1p expression levels are not altered in cells expressing globular tail-lacking Myo4p Defective control of asymmetric HO-endonuclease expression could be a result of impaired localization and localized translation of ASH1 mRNA. However, it could also be explained by corrupted translational silencing during otherwise intact transport. It has been described that premature ASH1-mRNA

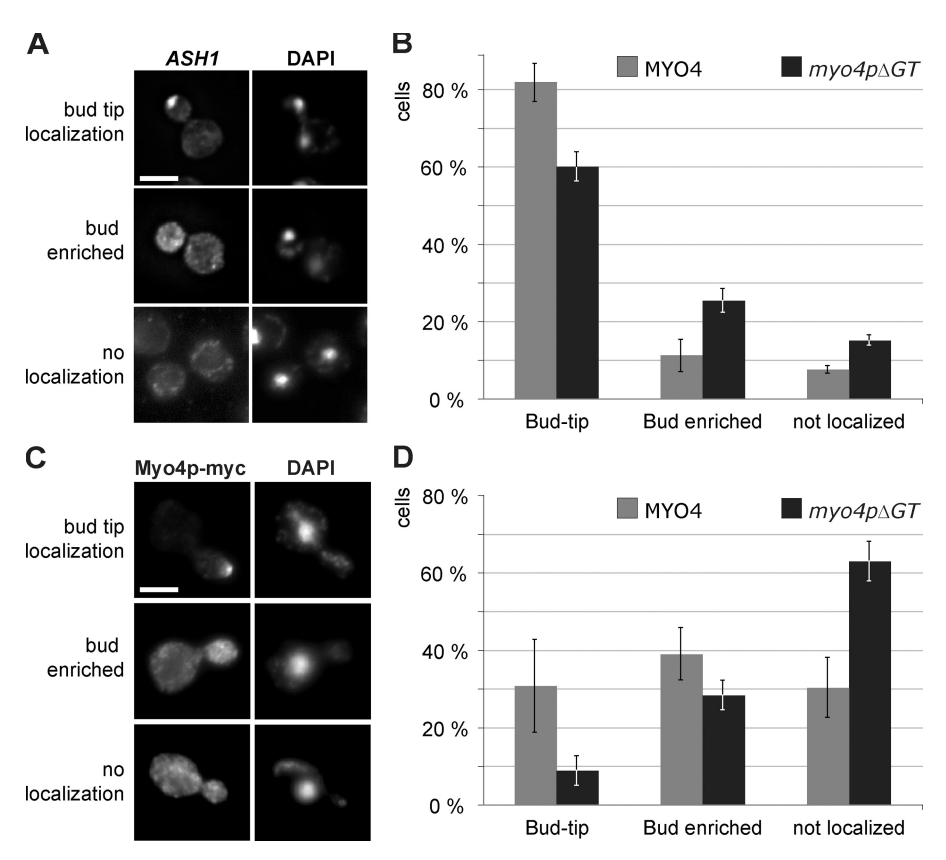


Figure 3. Myo4p globular tail is required for efficient ASH1 mRNA and Myo4p localization. (A) Representative images of mitotic yeast cells stained for ASH1 mRNA localization by fluorescent in situ hybridization (FISH, left images) and for nuclei by DAPI (right). (B) Graphical representation of the ASH1 mRNA distribution. Error bars represent the SD from three independent experiments of $n = 3 \times 270$ cells. The observed differences in bud-tip localization are statistically significant (two-sided t test; significance level P = 0.05). (C) Representative images of yeast cells with mid-sized buds that were stained for Myo4p-myc9 (left). Images on the right show DAPI staining. (D) Graphical representation of the Myo4p distribution. Error bars represent the SD from three independent experiments of $n = 3 \times 250$ cells. Bar (A and C): 4 μm.

translation before anchoring at the bud-tip results in increased Ash1p levels (Gu et al., 2004; Paquin et al., 2007; Du et al., 2008). Thus, if deletion of the globular tail impairs translational repression during transport, we should detect increased expression levels of Ash1p. When we compared the level of Myc-tagged Ash1p by Western blot in $myo4\Delta GT$ and in wild-type cells (MYO4), no significant difference was observed (1.07 \pm 0.03-fold of wild-type level; Fig. 2, C and D). This result rather argues against premature ASH1 translation upon deletion of the Myo4p globular tail.

The Myo4p globular tail is required for efficient localization of ASH1 mRNA

To test if a lack of the Myo4p globular tail affects bud-tip localization of ASH1 mRNA, we generated yeast strains that express Myc-tagged Myo4p or Myc-tagged Myo4p-ΔGT at comparable levels, as confirmed by Western blot analysis (Fig. S1 F). ASH1 mRNA localization was assessed in dividing cells by in situ hybridization (Fig. 3 A). In cells expressing wild-type Myo4p, $81.7 \pm 4.1\%$ of the cells localized the transcript at the bud tip, $11.1 \pm 3.8\%$ in the bud (i.e., bud enriched), and $7.3 \pm 0.6\%$ of the cells showed no localization (Fig. 3 B). In contrast, in Myo4p- Δ GT-expressing cells only 60.0 \pm 4.4% of the cells localized ASH1 mRNA at the bud tip, $25.3 \pm 3.2\%$ showed bud enrichment, and $14.7 \pm 1.2\%$ yielded no localization (Fig. 3 B). Cells lacking Myo4p expression showed no ASH1 mRNA localization (0.0%, not depicted; Long et al., 1997; Takizawa et al., 1997). In summary, the results suggest that the defective control of HO expression (Fig. 2, A and B) is caused by impaired ASH1 mRNA localization at the bud tip.

The globular tail is required for correct Myo4p localization at the bud tip

We also assessed whether Myc-tagged Myo4p- Δ GT-expressing cells show defects in localization of the motor itself. Myo4p localization was assessed in dividing cells by indirect immunofluorescense microscopy against the Myc tag (Fig. 3 C). In wild-type cells the motor localized at the bud tip in $30.7 \pm 12.0\%$ of all cells and showed a bud-enriched localization in $39.1 \pm 6.8\%$ (Fig. 3 D). In contrast, $myo4p\Delta GT$ cells showed an impaired motor localization with only $8.8 \pm 3.8\%$ bud tip localization and $28.3 \pm 3.8\%$ bud enrichment (Fig. 3 D). Thus, the deletion of the Myo4p globular tail also impairs the localization of the motor itself.

Structural analysis of the Myo4p globular tail

The globular tail of Myo4p binds its cargo only in concert with the protease-sensitive linker and the more N-terminal coiled coil—containing region (Heuck et al., 2007; Hodges et al. 2008), whereas in the paralogue Myo2p cargo binding is mediated by the globular tail itself (Weisman, 2006). For the globular tail of Myo2p, a high-resolution structure is available (Pashkova et al., 2006). We reasoned that structural information on the Myo4p globular tail would help to understand the function of this motor protein and that its comparison with the Myo2p structure should provide a sense for the structural conservation among type V myosins. Because both globular tails share only 25% identical amino acids (Fig. S2) and because such a low sequence conservation is insufficient to generate trustworthy structural models (Xiang, 2006), we determined the structure of the Myo4p globular tail by x-ray crystallography.

Table I. Data collection and refinement statistics

| Data collection | | | Refinement | | |
|---------------------|---------------|---------------|------------------------|----------|--|
| Data set | Native | SeMet K Peak | | | |
| x-ray source | ID14-2 (ESRF) | X12 (DESY) | | | |
| Wavelength (Å) | 0.933 | 0.978 | Data range (Å) | 96.0-2.3 | |
| Data range (Å) | 96-2.3 | 20–3.2 | Reflections F > 0 | 36,093 | |
| Observations | 286,493 | 202,888 | R_{work} | 0.254 | |
| (unique) | (35,353) | (26,406) | (R _{free}) | (0.287) | |
| l/σl | 13.2 | 18.3 <i>7</i> | RMS bond length (Å) | 0.030 | |
| (last shell) | (4.88) | (6.85) | RMS bond angles (deg) | (2.170) | |
| Completeness (%) | 98.1 | 98.5 | Ramachandran plot (%) | | |
| (last shell) | (94.7) | (95.7) | (allowed) | 95.4 | |
| | | | (additionally allowed) | 4.4 | |
| R _{sym} | 0.06 | 0.11 | • | | |
| (last shell) | (0.38) | (0.29) | | | |
| R _{Cullis} | _ | 0.823 | | | |
| Phasing power | _ | 1.024 | | | |
| Figure of merit | _ | 0.362 | | | |

Cell symmetry: $(P2_12_12_1)$ cell constants (\mathring{A}) : $\alpha = 43.46$, b = 120.99, c = 157.68. R_{sym} is the unweighted R-value on I between symmetry mates. $R_{work} = \Sigma_{hkl}$ II $F_{obs}(hkl)$ I -10^{-10} for reflections in the working data set. $R_{free} = 10^{-10}$ cross validation R-factor for 5% of reflections against which model was not refined. $R_{Cullis} = \frac{1}{R_{Culc}} \frac{1}{$

Crystals grown from the Myo4p globular tail (see Materials and methods) showed high-quality diffraction to 2.3 Å resolution. Because our attempts to obtain phase information by molecular replacement with the globular tail of Myo2p (RCSB Protein Databank ID: 2F6H) as the template failed, we determined the structure by single-wavelength anomalous diffraction using crystals from selenomethionine-derivatized proteins (Table I). The structure of the Myo4p globular tail ($R_{work} = 25.4\%$; $R_{free} = 28.7\%$) includes aa 1101–1468 and lacks disordered loop regions from residues 1208–1213, 1400–1402, and 1446–1457, as well as the very N-terminal 10 and C-terminal 11 residues.

The structure of the Myo4p globular tail has a hook-like shape and is mainly composed of amphipathic α -helices (Fig. 4 A). It is organized in two globular subdomains, each consisting of an α -helical bundle (Fig. 4, B and C). Subdomain I reaches from helix H1 to the first half of helix H6. Subdomains I and II are connected by helix H6, which participates with its C-terminal half also in the globular core of subdomain II (Fig. 4, A–C). In addition, subdomain II comprises a three-helical extension (H11 to H13). From helix H13 the peptide chain loops back along the entire structure to the N terminus, where the C-terminal helix H14 interacts with helices H1 and H2 at the tip of subunit I. A plot of the electrostatic surface potential of the Myo4p globular tail reveals no extensive surface areas with pronounced charges or large hydrophobic patches (Fig. 4 D).

Myo4p globular tail shows structural similarity to Myo2p and to components of three distinct membranetethering complexes

The crystal structures of the globular tail domains from Myo4p and Myo2p show similar overall folds (Fig. S3, A–E). However, the orientation of subdomains I and II relative to each other are different and result in a comparably large root-mean-square

deviation (RMSD) of 8.4 Å for their helical regions. Despite their different relative orientations, the individual subdomains I and II from Myo2p and Myo4p have almost identical geometries (Fig. S3, B and C) and RMSD values of 1.5 Å and 3 Å, respectively.

A database search also yielded strong similarity to components of three multi-subunit membrane-tethering complexes (Fig. S3, F-J). This similarity includes the factors Sec6p (PDB-ID: 2FJI, Z-score: 16.0; Sivaram et al., 2006), Sec15p (PDB-ID: 2A2F, Z-score: 11.3; Wu et al., 2005), and Exo70p (PDB-ID: 2B1E, Z-score: 9.2; Dong et al., 2005) from the exocyst complex, as well as Dsl1p from the Dsl1 membrane tethering complex (PDB-ID: 3K8P, Z-score: 13.8; Ren et al., 2009), and the conserved oligomeric 4 (COG4) factor of the COG complex (PDB-ID: 3HR0, Z-score: 11.1; Richardson et al., 2009). Weaker structural similarity was also observed to the exocyst component Exo84p (not depicted; PDB-ID: 2D2S, Z-score: 4.6) and the ER-associated factor GET4 (not depicted; PDB-ID: 2WPV; Z-score: 6.1). The role of these factors in membrane tethering and the localization of exocyst components at the bud tip in yeast (Ungar et al., 2006; Wu et al., 2008; He and Guo, 2009) suggests that globular tails of type V myosins could also be involved in the tethering of motors to membranes.

The globular tail of Myo4p lacks a previously described motif for motor auto-inhibition

One common property of type V myosins is the auto-inhibition of the motor domain by their C-terminal globular tails (Li et al., 2006; Liu et al., 2006; Thirumurugan et al., 2006; Ikebe, 2008). Based on experiments with a heterologous fusion protein, a globular tail–dependent motor inhibition was also proposed for Myo4p (Hodges et al., 2008). However, because Myo4p itself is monomeric (Dunn et al., 2007; Heuck et al., 2007; Hodges et al., 2008) and may require oligomerization

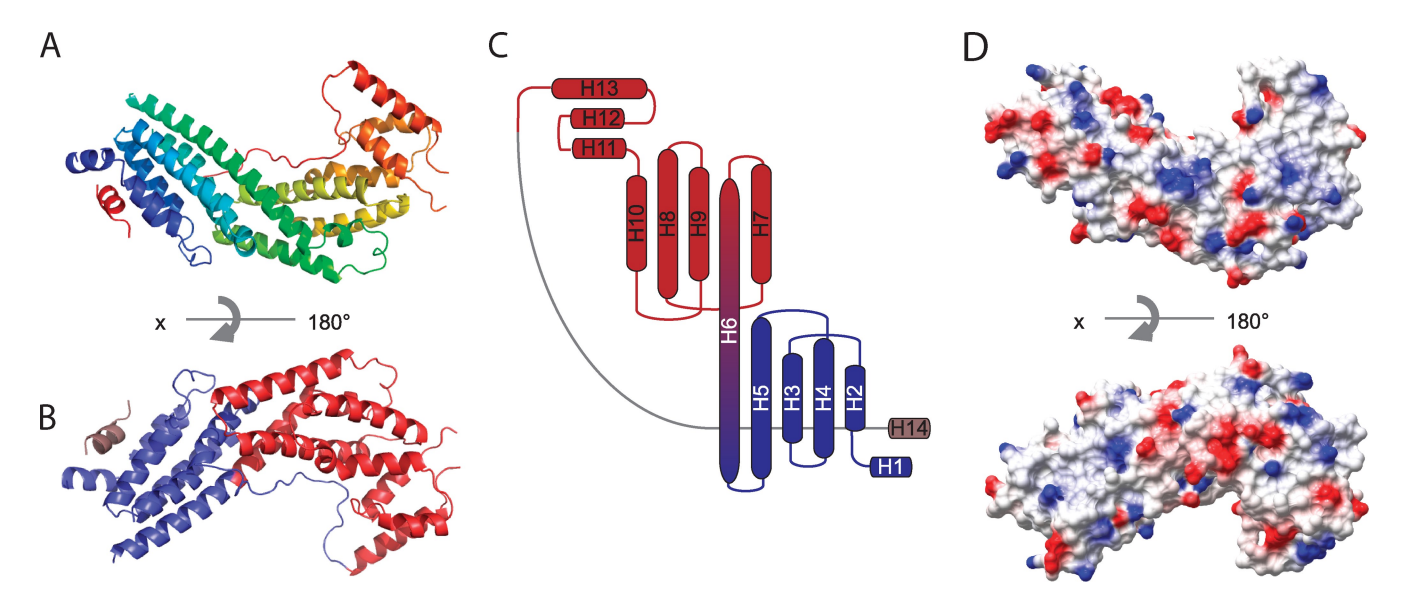


Figure 4. Crystal structure of the Myo4p globular tail. (A) Cartoon representation of the Myo4p globular tail structure, colored in rainbow representation with the N terminus in blue and C terminus in red. The N and C termini are located next to each other. (B) The Myo4p globular tail, rotated by 180° around the x axis. Subdomain I is highlighted in blue and sub-domain II in red. (C) Topogram of the Myo4p globular tail structure. Colors are the same as in B, except for the loop-connecting helices H13 and H14, which are represented in gray. (D) Surface charge representation of the Myo4p globular tail, with positively and negatively charged areas shown in blue and red, respectively. Cartoon representations were generated with PyMOL (DeLano Scientific LLC), surface charges with CCP4mg (Potterton et al., 2002).

for processive movement (Dunn et al., 2007; Heuck et al., 2007), it was also questioned if globular tail—dependent auto-inhibition is indeed used by Myo4p (Heuck et al., 2007). In contrast to Myo2p, the structure of the Myo4p globular tail reveals that surface residues involved in auto-inhibition of type V myosins (Li et al., 2008) are neither conserved in Myo4p or its orthologues (Fig. S4), nor are they substituted by nearby residues with similar chemical properties (Fig. 5 A). Thus, the absence of an auto-inhibition motif renders the known globular tail—dependent inhibition for Myo4p unlikely.

Overall sequence conservation of Myo4p

The alignment of the protein sequences (Fig. S2) revealed a low overall conservation between the tails of Myo4p and Myo2p, especially in regions involved in cargo binding by Myo2p (not depicted; Pashkova et al., 2006). A plot of the sequence alignment from Myo4p, Myo2p, and the human Myo5a (Fig. S2) onto the structure of the Myo4p globular tail (Fig. 5 B) yielded very little sequence conservation at the surface (3.5% identity; Fig. 5 C). In contrast, 11.3% of the buried amino acids are identical in all three type V myosins. The lower than average conservation at the surface might be a direct consequence of the different requirements for cargo binding of these motor proteins.

A sequence alignment of the Myo4p globular tail with respective regions of its Myo4p orthologues from *Saccharomyces castellii* and *Candida glabrata* (Fig. S4) and a subsequent surface plot of the alignment onto the Myo4p globular tail structure (Fig. S5 A) yielded surface areas of higher sequence conservation. In general, subdomain II showed a higher surface conservation than subdomain I (Fig. S4: compare residues 1101–1245 with residues 1270–1445; Fig. S5 A). On the surface plot, we recognized a conserved patch in subdomain II with surface-exposed tryptophane and tyrosine residues (Fig. S5, B and C).

Point mutations in the globular tail impair She3p interaction in vitro

Because tryptophans and tyrosines on protein surfaces have been reported to have an above average probability to participate in stable protein–protein interactions (Jones and Thornton, 1996), we reasoned that they may play a functional role in She3p association. To test whether this surface patch is important for She3p interaction, we generated a Myo4p globular tail with tryptophan in position 1325 and tyrosine in position 1329 substituted with glutamic acid (GST-Myo4p-L-GT-(W1325D, Y1329D); Fig. 6 A). We also generated a second double mutant in close proximity to the described patch, where we exchanged the two surface-exposed hydrophobic residues leucine in position 1365 and isoleucine in position 1367 against glycine (GST-Myo4p-L-GT-(L1365G, I1367G); Fig. 6 A and Fig. S5, B and C). Correct folding of both double mutants was assessed by size-exclusion chromatography and circular dichroism spectroscopy (Fig. S5 D).

To test whether these mutants are important for the binding of Myo4p to She3p, we repeated pull-down experiments with GST-Myo4p-L-GT and the mutated derivatives of this fragment. Whereas GST-Myo4p-L-GT showed the expected strong interaction (Fig. 6 B; see also Fig. 1, B, F, and G), neither GST-Myo4p-L-GT-(W1325D, Y1329D) nor GST-Myo4p-L-GT-(L1365G, I1367G) yielded any detectable binding in pull-down experiments (Fig. 6 B). Thus, both point mutants impair the interaction with She3p in vitro, providing additional evidence that the globular tail is important for She3p binding.

Point mutations in the globular tail and in the linker region impair localization of ASH1 mRNA

Our in vitro pull-down experiments revealed that the double mutation F1056R, I1057R in the protease-sensitive linker region

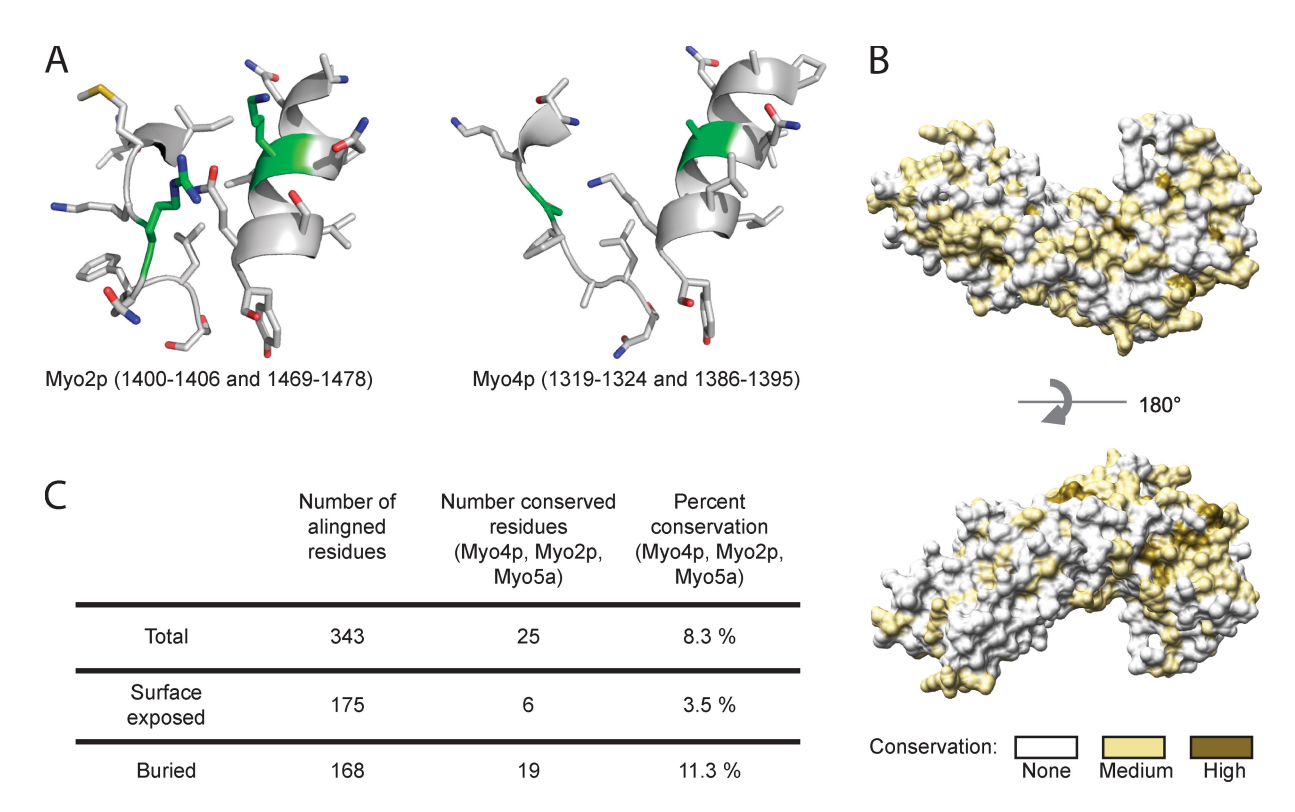


Figure 5. **Structural conservation of the globular tail of Myo4p.** (A) Residues involved in auto-inhibition of type V myosins by their globular tail (Li et al., 2008) are conserved in Myo2p (green residues, left) but not in Myo4p (green residues, right), suggesting a lack of auto-inhibition in Myo4p. (B) Surface plot of a sequence alignment from Myo4p, Myo2p, and human Myo5a (Fig. S2) show few regions with pronounced sequence identity. Dark yellow indicates residues identical in all three homologues, light yellow shows residues conserved in two homologues, and gray means no conservation. (C) Table showing that surface-exposed residues in Myo4p are much less conserved than buried residues, indicating a lack of conservation of potential binding surfaces.

(Fig. 1, A and E) and the double mutations in the globular tail (Fig. 6, A and B) impair the interaction with She3p. To test whether both types of mutations also impair ASH1 mRNA localization in vivo, we expressed plasmid-encoded full-length Myo4p with the respective double mutations in $myo4\Delta$ background in yeast and assessed ASH1 mRNA localization by in situ hybridization. In $78.9 \pm 6.5\%$ of the wild-type Myo4pexpressing cells the ASH1 mRNA was localized at the bud tip, whereas in 14.9 \pm 5.0% of these cells ASH1 mRNA accumulated in the bud $(6.0 \pm 1.7\%$ showed no localization; Fig. 6 C). Mutations in the Myo4p linker region (Myo4p-(F1056R, I1057R)) resulted in reduced bud tip and bud localization of the ASH1 mRNA (61.3 \pm 4.2% and 21.3 \pm 3.2%, respectively; $17.3 \pm 2.5\%$ showed no localization). This distribution is similar to the situation in cells with mutations in the globular tail (Myo4p-(W1325D, Y1329D)), which results in ASH1-mRNA localization at the bud tip in 55.7 \pm 2.1% of all cells (20.3 \pm 4.7% bud localization and $24.0 \pm 3.0\%$ without localization; Fig. 6 C). Cells transfected with an empty vector (mock control) did not localize ASH1 mRNA to the bud tip (not depicted). Although the experimental setup was not identical, the ASH1 mRNA localization defects observed with Myo4p-(F1056R, I1057R) and Myo4p-(W1325D, Y1329D) expressed from plasmids are similar to the defects observed for a genomically expressed Myo4p fragment lacking the entire globular tail (Fig. 3, A and B). In summary, these results confirm the defects in She3p binding and demonstrate that both the linker and the globular tail play a role in *ASH1* mRNA transport. The moderate defects are consistent with previous findings that She3p binding by this C-terminal interaction region is to some extent redundant with the more N-terminal coiled coil—containing interaction region (Heuck et al., 2007; Hodges et al., 2008).

Discussion

A recent study showed that the globular tail of Myo4p is not required for the localization of GFP-MS2–tethered particles to the bud and for the inheritance of ER (Bookwalter et al., 2009). This observation suggested that the globular tail might be dispensable for the localization of endogenous *ASH1* mRNA and thus also for inhibition of mating type switching in the daughter cell. It further raised the question of whether the globular tail of Myo4p has any function. Here, we used an experimentally refined, globular tail—lacking Myo4p to confirm the previous findings from Bookwalter et al. (2009) (Fig. S1, A–F).

However, when analyzing mother cell–specific expression of the HO endonuclease in cells expressing a globular tail–lacking Myo4p fragment, we found that this process is impaired (Fig. 2, A and B). The subsequent analysis of *ASH1* mRNA localization by in situ hybridization and of Myo4p localization by immunofluorescence staining consistently showed that the globular tail is required for full Myo4p activity in vivo (Fig. 3). In vitro interaction studies with different Myo4p fragments and its adapter She3p also demonstrated that the globular tail is required for

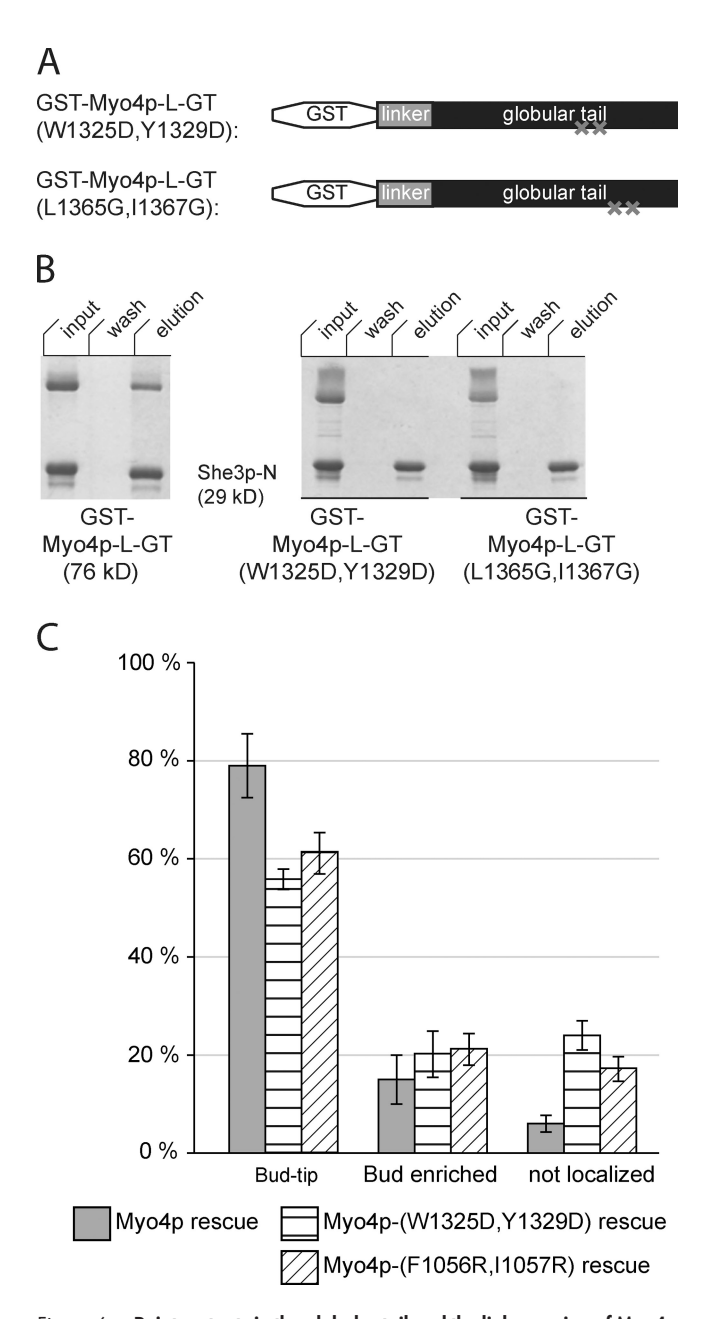


Figure 6. Point mutants in the globular tail and the linker region of Myo4p impair She3p binding and ASH1 mRNA localization. (A) Cartoon representation of Myo4p fragments containing point mutations. Representation is identical to Fig. 1 A. (B) Ni-sepharose pull-down reactions with immobilized His-She3p-N and point-mutated Myo4p fragments. Whereas both Myo4p fragments with double point mutations in their globular tail showed no detectable interaction (right), the same Myo4p fragment without point mutations yielded significant binding (left). (C) Graphical representation of the ASH1 mRNA localization in myo4∆ cells, rescued by the expression of either wild-type Myo4p or its mutant forms Myo4p-(W1325D,Y1329D) and Myo4p-(F1056R,I1057R). ASH1 mRNA localization is the same as in Fig. 3, A and B. Both mutants show statistically significant defects in bud-tip localization (two sided ±test; significance level P = 0.05). SDs are derived from three independent experiments of n = 3 x ≥50 cells (total >200 cells

efficient complex formation (Fig. 1 A,F,G). Analysis of surface features of the Myo4p globular tail and subsequent mutational studies identified a set of mutations in the globular tail that impairs She3p binding in vitro and reduces *ASH1* mRNA localization in vivo (Fig. 6 and Fig. S5, A–D). Furthermore, the

protease-sensitive linker between the coiled-coil region and the globular tail contains a hydrophobic sequence patch that, upon mutation, also results in impaired She3p binding and reduced *ASH1* mRNA localization (Fig. 1 E and Fig. 6 C). Thus, deletion studies as well as point mutations in the linker region and in the globular tail confirm the requirement of both regions for She3p binding and Myo4p function. An obvious question arising from these findings is why two independent groups (this study and Bookwalter et al., 2009) were unable to detect this localization defect by analyzing RNA localization with GFP-MS2–tethered particles.

It has been reported that insertion of MS2-stem loops into the 3' UTR of ASH1 mRNA and the tethering of multiple GFP-MS2 molecules to the 3' UTR reduces the number of ASH1 transport particles and increases their size (Bertrand et al., 1998; Lange et al., 2008). This effect is particularly pronounced when the reporter RNA is expressed from a strong GAL1 promoter. In the majority of cases, we detected only a single large particle per cell (see Fig. S1 D), whereas normal cells contain several ASH1-mRNA particles, even when ASH1 mRNA is overexpressed (Lange et al. 2008). In light of these considerations, our findings indicate that GFP-MS2-tethered particles may not always faithfully recapitulate endogenous ASH1 mRNA localization. This technical limitation might be particularly true for defects that do not result in a total loss of ASH1 mRNA localization, like the deletion of the globular tail studied here.

For ER inheritance, moderately impaired Myo4p-dependent transport may also not result in detectable differences. Certain aspects of Myo4p function differ for ASH1 mRNA localization function. For ASH1 mRNA localization, the motor Myo4p, full-length She3p, the RNA-binding protein She2p, as well as a number of additional RNA-binding factors are required; in contrast, Myo4p and the N-terminal domain of She3p are sufficient for ER inheritance (Estrada et al., 2003; Schmid et al. 2006). In addition, cortical ER is tethered to the Myo4p-She3p complex by an unknown mechanism and its inheritance does not seem to require an anchoring step at the bud tip. It has also been disputed how important the contribution of Myo4p to ER inheritance is (Reinke et al., 2004). Finally, it should be noted that ER inheritance is happening early in the cell cycle, before ASH1 mRNA is expressed and localized. In summary, there are several differences between ER inheritance and ASH1 mRNA localization that could explain the lacking defect in ER inheritance. More molecular details of ER inheritance may be required to understand the mechanistic basis of this difference.

The x-ray structure of the Myo4p globular tail revealed an almost entirely α -helical domain with a hook-like arrangement. The sequence identity between the globular tails of Myo4p and Myo2p is only 25% (Fig. S2). It is therefore remarkable that both domains share a very similar structural arrangement, composed of two almost identical subdomains. Considering the very different functions of Myo2p and Myo4p, and the low sequence identity for their globular tails, it is possible that similar domain architectures are also present in globular tail domains of other type V myosins. The extremely low surface conservation indicates that these domains evolved significantly diverging surface

properties to allow for the binding of very different cargoes or cargo adapters.

However, when superposing the globular tails of Myo4p and Myo2p, we found that the surface region of Myo4p required for She3p binding (Fig. S5, B and C) overlaps with residues in Myo2p important for peroxisome inheritance and interaction with its peroxisome cargo adapter Inp2p. (Fig. S5, E and F; Fagarasanu et al., 2009). This surface is also required for the interaction of Myo2p with the Rab GTPases Ypt31/32 and motility of endocytic compartments (Lipatova et al., 2008). These structural overlaps suggest that at least some type V myosins might have a common functional site in their globular tail, albeit with different cargo specificities.

Our structural analyses also revealed that the Myo4p globular tail lacks residues conserved in other MyoV motors (Fig. 5 A; Figs. S2 and S4) that are required for auto-inhibition of their motor domains. The lacking conservation of this surface area suggests that Myo4p does not undergo auto-inhibition by the previously described mechanism (Li et al., 2008). Because Myo4p is strictly monomeric in absence of cargo complexes (Dunn et al., 2007; Heuck et al., 2007; Hodges et al., 2008) and may require oligomerization for processive movement (Dunn et al., 2007; Heuck et al., 2007), such an auto-inhibition mechanism might indeed not be required.

Database searches yielded strong structural similarity of the globular tails of Myo4p and Myo2p to components of the membrane-tethering exocyst, Dsl1 and COG complexes (Fig. S3, D–I). The role of these factors in membrane tethering and the localization of exocyst components at the bud tip in yeast (Ungar et al., 2006; Wu et al., 2008; He and Guo, 2009) suggest that MyoV globular tails could potentially also tether to membrane sites.

All exocyst components with known structures share a similar overall fold (Munson and Novick, 2006). Because these exocyst components are thought to interact with each other through their elongated helical bundles (Dong et al., 2005), a similar interaction with exocyst components could also be envisioned for the structurally related MyoV globular tails. However, immunoprecipitation experiments with the globular tail of Myo4p failed to yield an interaction with the exocyst components Sec3p, Sec5p, Sec6p, Sec10p, Sec15p, Exo70p, or Exo84p above background levels (unpublished data). Because interaction studies with membrane-associated complexes are often technically demanding, it might be that experimental limitations prevented us from detecting binding to the exocyst complex. More thorough experiments will be required to rigorously assess the functional relationship of exocyst components and the Myo4p globular tail.

Regardless of this preliminary result, it will be interesting to see if globular tails of other MyoV motors can interact with exocyst components. The most pronounced difference between the Myo2p and Myo4p globular tails is the relative arrangement of their subdomains I and II and their resulting different overall shapes. In case a subset of MyoV globular tails indeed binds to exocyst components, such a difference in subdomain orientation could influence their propensity to interact with the elongated helical bundles of the exocyst complex.

In type V myosins of higher eukaryotes, regions outside the globular tail also contribute to binding of cargo complexes (Li and Nebenführ, 2008). For instance, vertebrate Myo5a interacts with its adapter melanophilin through the globular tail and a more N-terminal motif in the rod region (Wu et al., 2002). A second example is Myo5b, where also a motif in the rod and in the globular tail has been suggested to mediate binding to its Rab11-FIP2 cargo complex (Lapierre et al., 2001). These binding motifs outside the globular tail are only found in alternatively spliced, tissue-specific versions of Myo5a/b, whereas their other splice forms bind to different cargo complexes (Li and Nebenführ, 2008). In yeast, Myo2p and Myo4p exist only as a single isoform. Based on sequence identity (Fig. S2 B), dimerization state (Dunn et al., 2007; Heuck et al., 2007; Hodges et al., 2008), and the presence of an auto-inhibition motif in the globular tail (Fig. 5 A), Myo2p is arguably the closer homologue to MyoV from vertebrates. However, only Myo4p binds its cargo in a way reminiscent of the alternatively spliced Myo5a and Myo5b motors. In summary, we find that the generally assumed requirement of the globular tail in type V myosins for cargo binding also holds true for Myo4p from yeast.

Materials and methods

Yeast strains

General methods to culture and manipulate yeast strains were performed as described previously (Gietz and Schiestl, 1991; Adams et al., 1997; Gietz and Sugino, 1988). All strains were derived from Y18 (Schmid et al., 2006), Y28 (Jansen et al., 1996), or Y56 (Bobola et al., 1996) either by transformation with the corresponding plasmids or homologous recombination (Janke et al., 2004). Detailed information on strains and plasmids is provided in Tables II–IV.

Yeast growth conditions

For ER and motor localization, cells were grown in the appropriate selective minimal medium (Adams et al., 1997). For the assessment of asymmetric Ash 1 p distribution or of localization of ASH1 mRNPs, cells were plated on appropriate selective minimal medium containing 5 mg/l adenine, 4% glucose or 2% raffinose and 80 mg/ml methionine, respectively. Expression of MS2-tagged ASH1 mRNAs was induced by diluting cells in selective medium containing 2% galactose and subsequent growth for 1 h. For induction of the GFP-\(\text{NP-peptide}\) expression, cells were washed with selective medium lacking methionine and incubated for one additional hour.

FISH and indirect immunofluorescence

FISH against ASH1 mRNA with digoxigenin-labeled antisense RNA and indirect immunofluorescence against myc-tagged Myo4p was performed as described in Münchow et al. (1999). After mounting in 80% glycerol, cells were inspected using a CellObserver epifluorescence microscope (Carl Zeiss, Inc.) equipped with a Lambda DG-4 light source (Sutter Instrument Co.) and a PZ2000 piezo-driven stage (Applied Scientific Instruments). Images were acquired with a CCD camera (MRm Rev.3; Carl Zeiss, Inc.) controlled by AxioVision 4.7 software (Carl Zeiss, Inc.). For each cell, image stacks of 30 images at a 0.2-µm distance were acquired. Stacks were subsequently processed to remove out-of-focus haze using the integrated deconvolution software package of the AxioVision software. After deconvolution, the 20 central images were projected into one plane.

Immunofluorescence microscopy

Indirect immunofluorescence against Myc-tagged proteins was essentially performed as described previously (Böhl et al., 2000; Kruse et al., 2002). Spheroplasts were sequentially incubated with mouse anti-Myc antibody (Roche) and goat anti-mouse IgG coupled to Alexa Fluor 594 (Invitrogen). Nuclei were stained with Hoechst stain solution (Sigma-Aldrich) and cells were mounted in 80% glycerol. For visualization of

Table II. Plasmids

| Name | Insert | Vector | Template | Primer | Enzyme | Source |
|---------------|---|-----------|------------------------|-----------------------|---------------------|--------------------------|
| E. coli expre | ssion | | | | | |
| P2 | She3p-N | pET 28a | genomic DNA | 06/07 | BamH1-Xho1 | (Heuck et al., 2007) |
| P7 | Myo4p tail | pGEX-6P-1 | genomic DNA | 02/04 | BamH1-Xho1 | (Heuck et al., 2007) |
| P10 | Myo4p-L-GT | pGEX-6P-1 | genomic DNA | 05/04 | BamH1-Xho1 | This study |
| P22 | Myo4p-GT | pGEX-6P-1 | genomic DNA | 013/04 | BamH1-Xho1 | This study |
| P21 | Myo4p-L _{1/2} -GT | pGEX-6P-1 | P10 | 014/04 | BamH1-Xho1 | This study |
| P134 | Myo4p tail (F1056R, 11057R) | pGEX-6P-1 | genomic DNA | O2/O4/ O98/O99 | Nde1-Spe1 | This study |
| P201 | GST-Myo4p-L- Myo2p-GT | pGEX-6P-1 | genomic DNA | O5/O86/ O252/O253 | BamH1-Xho1 | This study |
| P204 | GST-Myo4p-L | pGEX-6P-1 | genomic DNA | 05/0251 | BamH1-Xho1 | This study |
| P205 | GST-Myo4p-L- GT _{W1325D,Y1329D} | pGEX-6P-1 | genomic DNA | O5/O4/ O165/O166 | BamH1-Xho1 | This study |
| P206 | GST-Myo4p-L- GT _{L1365G-l1367G} | pGEX-6P-1 | genomic DNA | O5/O4/ O258/O259 | BamH1-Xho1 | This study |
| Yeast transfo | ormation | | | | | |
| P45 | p414-GAL1-Myo4 922-1472 | | | | | (Heuck et al., 2007) |
| P46 | YCp22 | | | | | (Gietz and Sugino, 1988) |
| P137 | Муо4р | YCp22 | genomic DNA and P45 | O4/O110/ O132/O134 | Kpn1-Hind3- Spe1 | This study |
| P145 | Myo4p-w1325D,Y1329D- | YCp22 | P137 | 098/099 | · | This study |
| P179 | Myo4p-F1056R, 11057R | YCp22 | P137 | 0165/0166 | | This study |
| P194 | pUG34-yeGFP3- 2xNLS-lambda | • | | · | | (Lange et al., 2008) |
| P195 | p414 GAL1-ASH1- 6xBoxB | | | | | (Lange et al., 2008) |

GFP fusion proteins, cells were fixed with paraformaldehyde. Cells were inspected at room temperature with a 100 NA 1.3 DIC oil objective using either a fluorescence microscope (model BX60; Olympus) with a CCD camera (ORCA ER; Hamamatsu Photonics) controlled by Openlab 4 software (PerkinElmer), or the Leica AF6000LX system (microscope, DMI6000 B; camera, DFC350FX; software: LAS AF). All localization experiments were performed three times by inspecting cells of medium-sized buds (2-ym diameter).

Western blot against Ash 1 p-Myc

Total protein was extracted from 10 OD_{600} units of logarithmically growing cells. After determination of the linear detection range of the antibodies and the cell lysates (Charette et al., 2010), 80 OD_{280} units of lysate were used for Western blot analysis of Ash1p-Myc with mouse anti-Myc antibody (Roche) and Pgk1p using mouse anti-Pgk1 antibody (Invitrogen). Signals were detected by chemiluminescence using a Fujifilm LAS-3000 mini system and integrated using the Multi Gauge software (Fujifilm) with background subtraction.

Protein purification and crystallization

GST-tagged myosin fragments and His-tagged She3p-N were expressed in *Escherichia coli* and isolated to a purity of $\geq\!95\%$ using standard chromatographic techniques (Heuck et al., 2007). GST tags were removed by protease cleavage (Müller et al., 2009), unless stated otherwise. Crystals were grown at 21°C by hanging-drop vapor-diffusion using a 1:1 mixture of protein (12–20 mg/ml) and crystallization solution containing 100 mM Hepes, pH 8.5, 20% PEG 3350, 150 mM HCO2Na, and 10 mM $K_2Pt(CN)_4$ for native crystals and 100 mM Hepes, pH 8.5, 20% PEG 3350, and 150 mM HCO2Na for selenomethionine (SeMet) substituted crystals. Crystals appeared within 24 h.

Structure determination

Cryoprotection was achieved by adding 20% ethylene glycol. Native data were recorded at ID14-1 (European Synchrotron Radiation Facility, France), integrated and scaled using Mosflm and SCALA (Collaborative Computational Project Number 4, 1994). Single-wavelength anomalous diffraction (SAD) experiments were recorded at beamline X12 (Deutsches

Elektronen-Synchrotron [DESY], Germany), integrated and scaled using XDS (Kabsch, 1993). 14 selenium atoms were located with SHELXD (Schneider and Sheldrick, 2002), phases obtained with SHARP (Bricogne et al., 2003), and extended to 2.3 Å. After partial automatic model building with ARP/wARP (Langer et al., 2008) the structure was manually completed using COOT (Emsley and Cowtan, 2004). Refinement was performed with Refmac (Murshudov et al., 1997; Terwilliger, 2002), using non-crystallographic symmetry. The final model was analyzed using SFCHECK. Protein Databank ID: 3MMI.

Ni pull-down

Pull-down experiments were essentially performed as described previously (Heuck et al., 2007). 50 µg of both proteins were incubated with 50 µl of Ni-Sepharose for 1 h in 20 mM Tris-HCl, pH 7.5, 200 mM NaCl, and 15 mM imidazole. Sepharose was washed five times with 200 µl reaction buffer, followed by a final wash step with 50 µl. Proteins were eluted with 50 µl buffer containing 20 mM Tris-HCl, pH 7.5, 200 mM NaCl, and 750 mM imidazole. For visualization, 1/10 of the input, 1/5 of the final wash, and 1/5 of the elution fraction was analyzed by SDS-PAGE and Coomassie staining.

Surface plasmon resonance

Experiments were performed using a Biacore 3000 system (GE Healthcare) with She3p-N bound to a CM5 chip surface (standard amine coupling: ≤200 RU). The Myo4p fragments were applied in running buffer (10 mM Hepes, pH 7.5, 200 mM NaCl, and 50 mM EDTA) with a concentration range from 1 µM to 10 µM.

Bioinformatics

Sequence alignments were performed with JPred (www.compbio.dundee .ac.uk/~www-jpred/) and visualized with the program CLC-free-workbench (CLCbia). Physical and chemical parameters of recombinant proteins were calculated with the program ProtParam, and the hydrophobicity prediction by the program ProtScale, using the Kyte–Doolittle amino acid scale. All programs are available via the ExPASy proteomics server (http://www.expasy.org/). Superposition of two homologous structures and RMSD calculation was performed with LSQMAN (http://xray.bmc.uu.se/usf/).

Table III. Oligonucleotides

| Name | Primer for biochemical characterization | | |
|------|---|--|--|
| O2 | 5' aaa gga tcc aag caa agg caa gag tac g 3' | | |
| O4 | 5^\prime aaa ctc gag tta ttt tct gtc taa ttt tat aat 3^\prime | | |
| O5 | 5' aaa gga tcc aga tta agt gat gaa gtc aaa 3' | | |
| O6 | 5' aaa gga tcc atg tcg gac cag gat aat acc 3' | | |
| 07 | 5' gga ctc gag tta ctt gct taa ttt tga 3' | | |
| O13 | 5' aaa gga tcc cta gtc aat gta att cgt aga 3' | | |
| 014 | 5' aaa gga tcc caa gat ttc acc acc aca tat 3' | | |
| O98 | 5' aag caa gaa cta gcg cga cga gaa aac gta ata 3' | | |
| 099 | 5' tat tac gtt ttc tcg tcg cgc tag ttc ttg ctt 3' | | |
| O86 | 5' gca ctc gag tta gtg gcc gtc ttg aac gac 3' | | |
| O110 | 5' cat ttg ttc aac ttg tgc cgt ctt cag ctt gga 3' | | |
| O132 | 5' aaa ggt acc ctg cag taa cag tta ggg cta ttc t 3' | | |
| O134 | 5' gcc gcg gcc gca agc tta aga cat agc aag cgc aac gta tt 3' | | |
| O165 | 5' tgt ccc gcg tta aat gat aag tat ggg gat gaa gtg gat aga aat 3' | | |
| O166 | 5^{\prime} att tot atc cac ttc atc ccc ata ctt atc att taa cgc ggg aca 3^{\prime} | | |
| O251 | 5' gca ctc gag tta ctt cgg ttt tac ttg ttg tcc 3' | | |
| O252 | 5' gac aac aag taa aac cga agg tcg atc gcg aaa atg gtg tc 3' | | |
| O253 | 5^\prime gac acc att ttc gcg atc gac ctt cgg ttt tac ttg ttg tc 3^\prime | | |
| O258 | 5' gtc aag ata tta cag gga aag gga agc aac ttg aac gag 3' | | |
| O259 | 5^\prime ctc gtt caa gtt gct tcc ctt tcc ctg taa tat ctt gac 3^\prime | | |
| Name | Primer used for homologous recombination in yeast | | |
| O195 | 5' atg ata aag tga aag gtt tgg gaa tcg cag gac aac aag taa aac cga agc gta cgc tgc agg tcg ac 3' | | |
| O196 | 5' ata cag agg gct tag cta ctg tag taa aat tat aaa att aga cag aaa acg tac gct gca ggt cga c $3'$ | | |
| O197 | 5' tat atg tat ata tac ata tat aca tat atg ggc gta tat tta ctt tgt tca tcg atg aat tcg agc tcg $3'$ | | |
| O208 | 5' ttg atg ttg tcg cta cta aat ggc atg aca aat ttg gta aat tga aaa acc gta cgc tgc agg tcg ac 3' | | |
| O209 | 5' tat taa cta gtg gta ctt att tgc tct ttt tga gct aaa aac tga agg cca tcg atg aat tcg agc tcg 3' | | |

Table IV. Yeast strains

| Strain | Essential genotype | Source |
|--------|---|-----------------------|
| Y18 | MAT a; URA3::HMG1-GFP | (Schmid et al., 2006) |
| Y21 | MAT α; URA3::HMG1-GFP; HIS3::MYO4-9Myc | This study |
| Y22 | MAT a: URA3::HMG1-GFP; HIS3::MYO4-1090stop-9Myc | This study |
| Y28 | MAT a; trp1-1; leu2-3; his3-11; ura3; ade2-1; HO-ADE2, HO-CAN1 | (Jansen et al., 1996) |
| Y29 | MAT a; trp1-1; leu2-3; his3-11; ura3; ade2-1; HO-ADE2, HO-CAN1, HIS3::MYO4-9Myc | This study |
| Y30 | MAT a; trp1-1; leu2-3; his3-11; ura3; ade2-1; HO-ADE2, HO-CAN1; HIS3::MYO4-1090stop-9Myc | This study |
| Y32 | MAT a; trp1-1; leu2-3; his3-11; leu; ura3; ade2-1; HO-ADE2, HO-CAN1; MYO4::URA3 | (Jansen et al., 1996) |
| Y35 | MAT a; trp1-1; leu2-3; his3-11; leu; ura3; ade2-1; HO-ADE2, HO-CAN1; MYO4::URA3; P46::TRP | This study |
| Y38 | MAT a; trp1-1; leu2-3; his3-11; leu; ura3; ade2-1; HO-ADE2, HO-CAN1; MYO4::URA3; P137::TRP | This study |
| Y39 | MAT a; trp1-1; leu2-3; his3-11; leu; ura3; ade2-1; HO-ADE2, HO-CAN1; MYO4::URA3; P179::TRP | This study |
| Y53 | MAT a; trp1-1; leu2-3; his3-11; ura3; ade2-1; HO-ADE2, HO-CAN1, CloNat::MYO4-9Myc, HIS:: P194, TRP:: P195 | This study |
| Y55 | MAT a; trp1-1; leu2-3; his3-11; ura3; ade2-1; HO-ADE2, HO-CAN1, CloNat::MYO4-1090stop-9Myc, HIS:: P194, TRP:: P195 | This study |
| Y56 | MAT a; trp1-1; leu2-3; his3-11; ura3; ade2-1; HO-ADE2, HO-CAN1, ASH1-myc9 | (Bobola et al. 1996) |
| Y58 | MAT a; trp1-1; leu2-3; his3-11; ura3; ade2-1; HO-ADE2, HO-CAN1, ASH1-myc9, CloNat::MYO4-1090stop-6HA | This study |
| Y59 | MAT a; trp1-1; leu2-3; his3-11; leu; ura3; ade2-1; HO-ADE2, HO-CAN1; MYO4::URA3; P145::TRP | This study |

Calculation and representation of the electrostatic surface was done with CCP4mg. Images of the crystal structures were prepared with PyMOL (DeLano Scientific LLC) and Chimera (Pettersen et al., 2004). t-test was performed with the program Statistica 7.1 (StatSoft).

Online supplemental material

Fig. S1 shows that the Myo4p globular tail is dispensable for ER inheritance and localization of MS2-GFP reporter particles. Fig. S2 contains a sequence alignment of different MyoV globular tails. Fig. S3 shows the structural similarity of the Myo4p globular tail to membrane-tethering complexes. Fig. S4 shows a sequence alignment of Myo4p orthologues from different yeast species. Fig. S5 shows structural details and mutations in the globular tails of Myo4p and Myo2p. Online supplemental material is available at http://www.jcb.org/cgi/content/full/jcb.201002076/DC1.

We are grateful to Sabine Heuck, Peter Hill, Sigrun Jaklin, Stephan Jellbauer, Susanne Lange, Gabriele Möller, Jacob Piehler, Maria Schmid, and Hana Velvarska for their contributions. We thank Katja Strässer for provision of the anti-Pgk1 antibody. We acknowledge EMBL/DESY and the European Synchrotron Radiation Facility for provision of synchrotron radiation facilities.

This work was supported by the Helmholtz Association (VG-NH $\,142$ to D. Niessing) and Deutsche Forschungsgemeinschaft (FOR855 to A. Heuck, R.-P. Jansen, and D. Niessing; SFB646 to R.-P. Jansen and D. Niessing).

Submitted: 15 February 2010 Accepted: 6 April 2010

References

- Adams, A., D.E. Gottschling, C.A. Kaiser, and T. Stearns. 1997. Methods in Yeast Genetics. Cold Spring Harbor Laboratory Press, Cold Spring Harbor, NY. 1–177.
- Bertrand, E., P. Chartrand, M. Schaefer, S.M. Shenoy, R.H. Singer, and R.M. Long. 1998. Localization of ASH1 mRNA particles in living yeast. Mol. Cell. 2:437-445. doi:10.1016/S1097-2765(00)80143-4
- Bobola, N., R.P. Jansen, T.H. Shin, and K. Nasmyth. 1996. Asymmetric accumulation of Ash1p in postanaphase nuclei depends on a myosin and restricts yeast mating-type switching to mother cells. Cell. 84:699-709. doi:10.1016/S0092-8674(00)81048-X
- Böhl, F., C. Kruse, A. Frank, D. Ferring, and R.P. Jansen. 2000. She2p, a novel RNA-binding protein tethers ASH1 mRNA to the Myo4p myosin motor via She3p. EMBO J. 19:5514-5524. doi:10.1093/emboj/19.20.5514
- Bookwalter, C.S., M. Lord, and K.M. Trybus. 2009. Essential features of the class V myosin from budding yeast for ASH1 mRNA transport. Mol. Biol. Cell. 20:3414-3421. doi:10.1091/mbc.E08-08-0801
- Bricogne, G., C. Vonrhein, C. Flensburg, M. Schiltz, and W. Paciorek. 2003. Generation, representation and flow of phase information in structure determination: recent developments in and around SHARP 2.0. Acta Crystallogr. D Biol. Crystallogr. 59:2023-2030. doi:10.1107/S0907444903017694
- Charette, S.J., H. Lambert, P.J. Nadeau, and J.J. Landry. 2010. Protein quantification by chemiluminescent Western blotting: elimination of the antibody factor by dilution series and calibration curve. J. Immunol. Methods. 353:148-150. doi:10.1016/j.jim.2009.12.007
- Collaborative Computational Project Number 4. 1994. The CCP4 suite: programs for protein crystallography. Acta Crystallogr. D Biol. Crystallogr. 50:760–763. doi:10.1107/S0907444994003112
- Dong, G., A.H. Hutagalung, C. Fu, P. Novick, and K.M. Reinisch. 2005. The structures of exocyst subunit Exo70p and the Exo84p C-terminal domains reveal a common motif. Nat. Struct. Mol. Biol. 12:1094-1100. doi:10.1038/nsmb1017
- Du, T.G., S. Jellbauer, M. Müller, M. Schmid, D. Niessing, and R.P. Jansen. 2008. Nuclear transit of the RNA-binding protein She2 is required for translational control of localized ASH1 mRNA. EMBO Rep. 9:781–787. doi:10.1038/embor.2008.112
- Dunn, B.D., T. Sakamoto, M.S. Hong, J.R. Sellers, and P.A. Takizawa. 2007. Myo4p is a monomeric myosin with motility uniquely adapted to transport mRNA. J. Cell Biol. 178:1193-1206. doi:10.1083/jcb.200707080
- Emsley, P., and K. Cowtan. 2004. Coot: model-building tools for molecular graphics. Acta Crystallogr. D Biol. Crystallogr. 60:2126–2132. doi:10.1107/S0907444904019158
- Estrada, P., J. Kim, J. Coleman, L. Walker, B. Dunn, P. Takizawa, P. Novick, and S. Ferro-Novick. 2003. Myo4p and She3p are required for cortical ER inheritance in Saccharomyces cerevisiae. J. Cell Biol. 163:1255-1266. doi:10.1083/jcb.200304030
- Fagarasanu, A., F.D. Mast, B. Knoblach, Y. Jin, M.J. Brunner, M.R. Logan, J.N. Glover, G.A. Eitzen, J.D. Aitchison, L.S. Weisman, and R.A. Rachubinski.

- 2009. Myosin-driven peroxisome partitioning in S. cerevisiae. J. Cell Biol. 186:541-554. doi:10.1083/jcb.200904050
- Gietz, R.D., and R.H. Schiestl. 1991. Applications of high efficiency lithium acetate transformation of intact yeast cells using single-stranded nucleic acids as carrier. Yeast. 7:253-263. doi:10.1002/yea.320070307
- Gietz, R.D., and A. Sugino. 1988. New yeast-Escherichia coli shuttle vectors constructed with in vitro mutagenized yeast genes lacking six-base pair restriction sites. Gene. 74:527–534. doi:10.1016/0378-1119(88)90185-0
- Gu, W., Y. Deng, D. Zenklusen, and R.H. Singer. 2004. A new yeast PUF family protein, Puf6p, represses ASH1 mRNA translation and is required for its localization. Genes Dev. 18:1452-1465. doi:10.1101/gad.1189004
- He, B., and W. Guo. 2009. The exocyst complex in polarized exocytosis. Curr. Opin. Cell Biol. 21:537-542. doi:10.1016/j.ceb.2009.04.007
- Heuck, A., T.G. Du, S. Jellbauer, K. Richter, C. Kruse, S. Jaklin, M. Müller, J. Buchner, R.P. Jansen, and D. Niessing. 2007. Monomeric myosin V uses two binding regions for the assembly of stable translocation complexes. Proc. Natl. Acad. Sci. USA. 104:19778-19783. doi:10.1073/ pnas.0706780104
- Hodges, A.R., E.B. Krementsova, and K.M. Trybus. 2008. She3p binds to the rod of yeast myosin V and prevents it from dimerizing, forming a singleheaded motor complex. J. Biol. Chem. 283:6906-6914. doi:10.1074/jbc .M708865200
- Ikebe, M. 2008. Regulation of the function of mammalian myosin and its conformational change. Biochem. Biophys. Res. Commun. 369:157-164. doi:10.1016/j.bbrc.2008.01.057
- Janke, C., M.M. Magiera, N. Rathfelder, C. Taxis, S. Reber, H. Maekawa, A. Moreno-Borchart, G. Doenges, E. Schwob, E. Schiebel, and M. Knop. 2004. A versatile toolbox for PCR-based tagging of yeast genes: new fluorescent proteins, more markers and promoter substitution cassettes. Yeast. 21:947-962. doi:10.1002/yea.1142
- Jansen, R.P., C. Dowzer, C. Michaelis, M. Galova, and K. Nasmyth. 1996. Mother cell-specific HO expression in budding yeast depends on the unconventional myosin myo4p and other cytoplasmic proteins. Cell. 84:687-697. doi:10.1016/S0092-8674(00)81047-8
- Jones, S., and J.M. Thornton. 1996. Principles of protein-protein interactions. Proc. Natl. Acad. Sci. USA. 93:13-20. doi:10.1073/pnas.93.1.13
- Kabsch, W. 1993. Automatic processing of rotation diffraction data from crystals of initially unknown symmetry and cell constants. J. Appl. Cryst. 26:795-800. doi:10.1107/S0021889893005588
- A. Jaedicke, J. Beaudouin, F. Böhl, D. Ferring, T. Güttler, J. Ellenberg, and R.P. Jansen. 2002. Ribonucleoprotein-dependent localization of the yeast class V myosin Myo4p. J. Cell Biol. 159:971-982. doi:10.1083/jcb.200207101
- Lange, S., Y. Katayama, M. Schmid, O. Burkacky, C. Bräuchle, D.C. Lamb, and R.P. Jansen. 2008. Simultaneous transport of different localized mRNA species revealed by live-cell imaging. Traffic. 9:1256-1267. doi:10.1111/ j.1600-0854.2008.00763.x
- Langer, G., S.X. Cohen, V.S. Lamzin, and A. Perrakis. 2008. Automated macromolecular model building for X-ray crystallography using ARP/wARP version 7. Nat. Protoc. 3:1171-1179. doi:10.1038/nprot.2008.91
- Lapierre, L.A., R. Kumar, C.M. Hales, J. Navarre, S.G. Bhartur, J.O. Burnette, D.W. Provance Jr., J.A. Mercer, M. Bähler, and J.R. Goldenring. 2001. Myosin vb is associated with plasma membrane recycling systems. Mol. Biol. Cell. 12:1843-1857.
- Li, J.F., and A. Nebenführ. 2008. The tail that wags the dog: the globular tail domain defines the function of myosin V/XI. Traffic. 9:290-298. doi:10.1111/j.1600-0854.2007.00687.x
- Li, X.D., H.S. Jung, K. Mabuchi, R. Craig, and M. Ikebe. 2006. The globular tail domain of myosin Va functions as an inhibitor of the myosin Va motor. J. Biol. Chem. 281:21789-21798. doi:10.1074/jbc.M602957200
- Li, X.D., H.S. Jung, Q. Wang, R. Ikebe, R. Craig, and M. Ikebe. 2008. The globular tail domain puts on the brake to stop the ATPase cycle of myosin Va. Proc. Natl. Acad. Sci. USA. 105:1140-1145. doi:10.1073/pnas.0709741105
- Lipatova, Z., A.A. Tokarev, Y. Jin, J. Mulholland, L.S. Weisman, and N. Segev. 2008. Direct interaction between a myosin V motor and the Rab GTPases Ypt31/32 is required for polarized secretion. Mol. Biol. Cell. 19:4177-4187. doi:10.1091/mbc.E08-02-0220
- Liu, J., D.W. Taylor, E.B. Krementsova, K.M. Trybus, and K.A. Taylor. 2006. Three-dimensional structure of the myosin V inhibited state by cryoelectron tomography. Nature. 442:208–211.
- Long, R.M., R.H. Singer, X. Meng, I. Gonzalez, K. Nasmyth, and R.-P. Jansen. 1997. Mating type switching in yeast controlled by asymmetric localization of ASH1 mRNA. Science. 277:383-387. doi:10.1126/ science.277.5324.383
- Müller, M., A. Heuck, and D. Niessing. 2007. Directional mRNA transport in eukaryotes: lessons from yeast. Cell. Mol. Life Sci. 64:171-180. doi:10.1007/s00018-006-6286-1

- Müller, M., K. Richter, A. Heuck, E. Kremmer, J. Buchner, R.-P. Jansen, and D. Niessing. 2009. Formation of She2p tetramers is required for mRNA binding, mRNP assembly, and localization. RNA. 15:2002–2012. doi: 10.1261/ma.1753309
- Münchow, S., C. Sauter, and R.-P. Jansen. 1999. Association of the class V myosin Myo4p with a localised messenger RNA in budding yeast depends on She proteins. *J. Cell Sci.* 112:1511–1518.
- Munson, M., and P. Novick. 2006. The exocyst defrocked, a framework of rods revealed. Nat. Struct. Mol. Biol. 13:577–581. doi:10.1038/nsmb1097
- Murshudov, G.N., A.A. Vagin, and E.J. Dodson. 1997. Refinement of macro-molecular structures by the maximum-likelihood method. Acta Crystallogr. D Biol. Crystallogr. 53:240–255. doi:10.1107/S0907444996012255
- Paquin, N., and P. Chartrand. 2008. Local regulation of mRNA translation: new insights from the bud. *Trends Cell Biol.* 18:105–111. doi:10.1016/j.tcb.2007.12.004
- Paquin, N., M. Ménade, G. Poirier, D. Donato, E. Drouet, and P. Chartrand. 2007. Local activation of yeast ASH1 mRNA translation through phosphorylation of Khd1p by the casein kinase Yck1p. *Mol. Cell.* 26:795–809. doi:10.1016/j.molcel.2007.05.016
- Pashkova, N., Y. Jin, S. Ramaswamy, and L.S. Weisman. 2006. Structural basis for myosin V discrimination between distinct cargoes. *EMBO J.* 25:693– 700. doi:10.1038/sj.emboj.7600965
- Pettersen, E.F., T.D. Goddard, C.C. Huang, G.S. Couch, D.M. Greenblatt, E.C. Meng, and T.E. Ferrin. 2004. UCSF Chimera—a visualization system for exploratory research and analysis. *J. Comput. Chem.* 25:1605–1612. doi:10.1002/jcc.20084
- Potterton, E., S. McNicholas, E. Krissinel, K. Cowtan, and M. Noble. 2002. The CCP4 molecular-graphics project. *Acta Crystallogr. D Biol. Crystallogr.* 58:1955–1957. doi:10.1107/S0907444902015391
- Reck-Peterson, S.L., D.W. Provance Jr., M.S. Mooseker, and J.A. Mercer. 2000. Class V myosins. *Biochim. Biophys. Acta.* 1496:36–51. doi:10.1016/ S0167-4889(00)00007-0
- Reinke, C.A., P. Kozik, and B.S. Glick. 2004. Golgi inheritance in small buds of Saccharomyces cerevisiae is linked to endoplasmic reticulum inheritance. Proc. Natl. Acad. Sci. USA. 101:18018–18023. doi:10.1073/ pnas.0408256102
- Ren, Y., C.K. Yip, A. Tripathi, D. Huie, P.D. Jeffrey, T. Walz, and F.M. Hughson. 2009. A structure-based mechanism for vesicle capture by the multisubunit tethering complex Dsl1. Cell. 139:1119–1129. doi:10.1016/j.cell.2009.11.002
- Richardson, B.C., R.D. Smith, D. Ungar, A. Nakamura, P.D. Jeffrey, V.V. Lupashin, and F.M. Hughson. 2009. Structural basis for a human glycosylation disorder caused by mutation of the COG4 gene. *Proc. Natl. Acad. Sci. USA*. 106:13329–13334. doi:10.1073/pnas.0901966106
- Schmid, M., A. Jaedicke, T.G. Du, and R.-P. Jansen. 2006. Coordination of endoplasmic reticulum and mRNA localization to the yeast bud. *Curr. Biol.* 16:1538–1543. doi:10.1016/j.cub.2006.06.025
- Schneider, T.R., and G.M. Sheldrick. 2002. Substructure solution with SHELXD.

 Acta Crystallogr. D Biol. Crystallogr. 58:1772–1779. doi:10.1107/S0907444902011678
- Sivaram, M.V., M.L. Furgason, D.N. Brewer, and M. Munson. 2006. The structure of the exocyst subunit Sec6p defines a conserved architecture with diverse roles. *Nat. Struct. Mol. Biol.* 13:555–556. doi:10.1038/nsmb1096
- Takizawa, P.A., A. Sil, J.R. Swedlow, I. Herskowitz, and R.D. Vale. 1997. Actin-dependent localization of an RNA encoding a cell-fate determinant in yeast. *Nature*. 389:90–93. doi:10.1038/38015
- Terwilliger, T.C. 2002. Automated structure solution, density modification and model building. *Acta Crystallogr. D Biol. Crystallogr.* 58:1937–1940. doi:10.1107/S0907444902016438
- Thirumurugan, K., T. Sakamoto, J.A. Hammer III, J.R. Sellers, and P.J. Knight. 2006. The cargo-binding domain regulates structure and activity of myosin 5. *Nature*. 442:212–215. doi:10.1038/nature04865
- Tsai, C.J., S.L. Lin, H.J. Wolfson, and R. Nussinov. 1997. Studies of proteinprotein interfaces: a statistical analysis of the hydrophobic effect. *Protein Sci.* 6:53–64.
- Ungar, D., T. Oka, M. Krieger, and F.M. Hughson. 2006. Retrograde transport on the COG railway. *Trends Cell Biol.* 16:113–120. doi:10.1016/j.tcb.2005.12.004
- Vale, R.D. 2003. The molecular motor toolbox for intracellular transport. Cell. 112:467–480. doi:10.1016/S0092-8674(03)00111-9
- Weisman, L.S. 2006. Organelles on the move: insights from yeast vacuole inheritance. Nat. Rev. Mol. Cell Biol. 7:243–252. doi:10.1038/nrm1892
- Wu, H., G. Rossi, and P. Brennwald. 2008. The ghost in the machine: small GTPases as spatial regulators of exocytosis. *Trends Cell Biol*. 18:397–404. doi:10.1016/j.tcb.2008.06.007
- Wu, S., S.Q. Mehta, F. Pichaud, H.J. Bellen, and F.A. Quiocho. 2005. Sec15 interacts with Rab11 via a novel domain and affects Rab11 localization in vivo. Nat. Struct. Mol. Biol. 12:879–885. doi:10.1038/nsmb987

- Wu, X.S., K. Rao, H. Zhang, F. Wang, J.R. Sellers, L.E. Matesic, N.G. Copeland, N.A. Jenkins, and J.A. Hammer III. 2002. Identification of an organelle receptor for myosin-Va. *Nat. Cell Biol.* 4:271–278. doi:10.1038/ncb760
- Xiang, Z. 2006. Advances in homology protein structure modeling. *Curr. Protein Pept. Sci.* 7:217–227. doi:10.2174/138920306777452312

m

Ш

JOURNAL

뽀

Supplemental material

JCB

Heuck et al., http://www.jcb.org/cgi/content/full/jcb.201002076/DC1

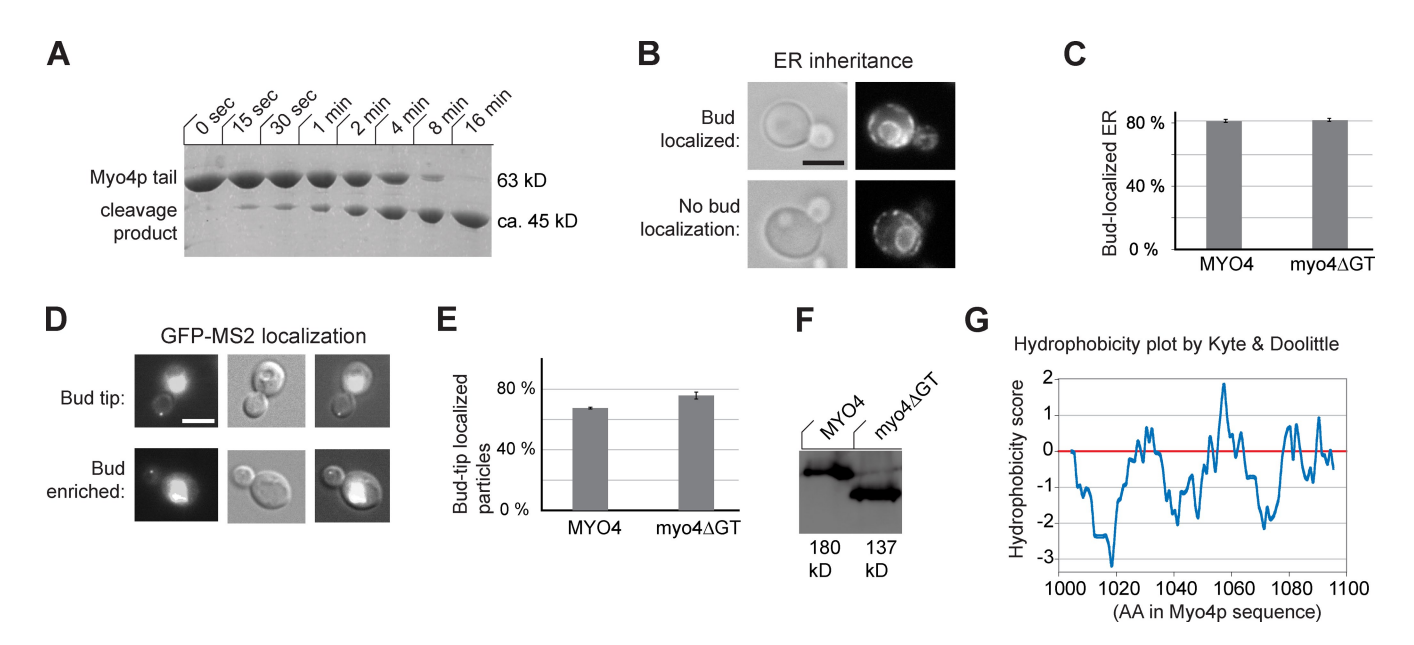


Figure S1. Characterization of the Myo4p tail and the role of the globular tail in ER inheritance and localization of GFP-MS2 particles. (A) Limited proteolysis of Myo4p tail (see Fig. 1 A) at room temperature with the protease Glu-C reveals a stable cleavage product of \sim 45 kD. (B and C) ER inheritance in cells expressing a globular tail-lacking Myo4p fragment ($myo4\Delta GT$) and in wild-type Myo4p-expressing cells (MYO4). (B) Representative images of ER inheritance in dividing yeast cells. Images were taken from Hmg1p-GFP-expressing yeast cells with transmission light (left) and fluorescence microscopy (right). (C) The amount of cells with bud-localized ER is indistinguishable between MYO4 cells and $myo4\Delta GT$ cells. Error bars represent SD from the analysis of $n = 3 \times \ge 80$ cells for each experiment. (D and E) Localization of GFP-MS2-tethered mRNPs in dividing yeast cells (Bertrand et al., 1998). (D) Representative images of cells localizing GFP-MS2 particle. Images were taken from GFP-expressing yeast cells with transmission light (left) and fluorescence microscopy (middle). Right image: overlay. (E) No considerable difference in bud-tip localization of GFP-MS2 particles was observed between MYO4 cells and $myo4\Delta GT$ cells. Error bars represent SD from the analysis of $n = 3 \times \ge 100$ cells for each experiment. (F) Western blot showing that expression levels are comparable between wild-type Myo4p and Myo4p with deleted globular tail. (G) Hydrophobicity plot of the protease-sensitive linker region of the Myo4p linker region indicates an accumulation of hydrophobic residues around position 1060. Bar (B and D): 4 μ m.

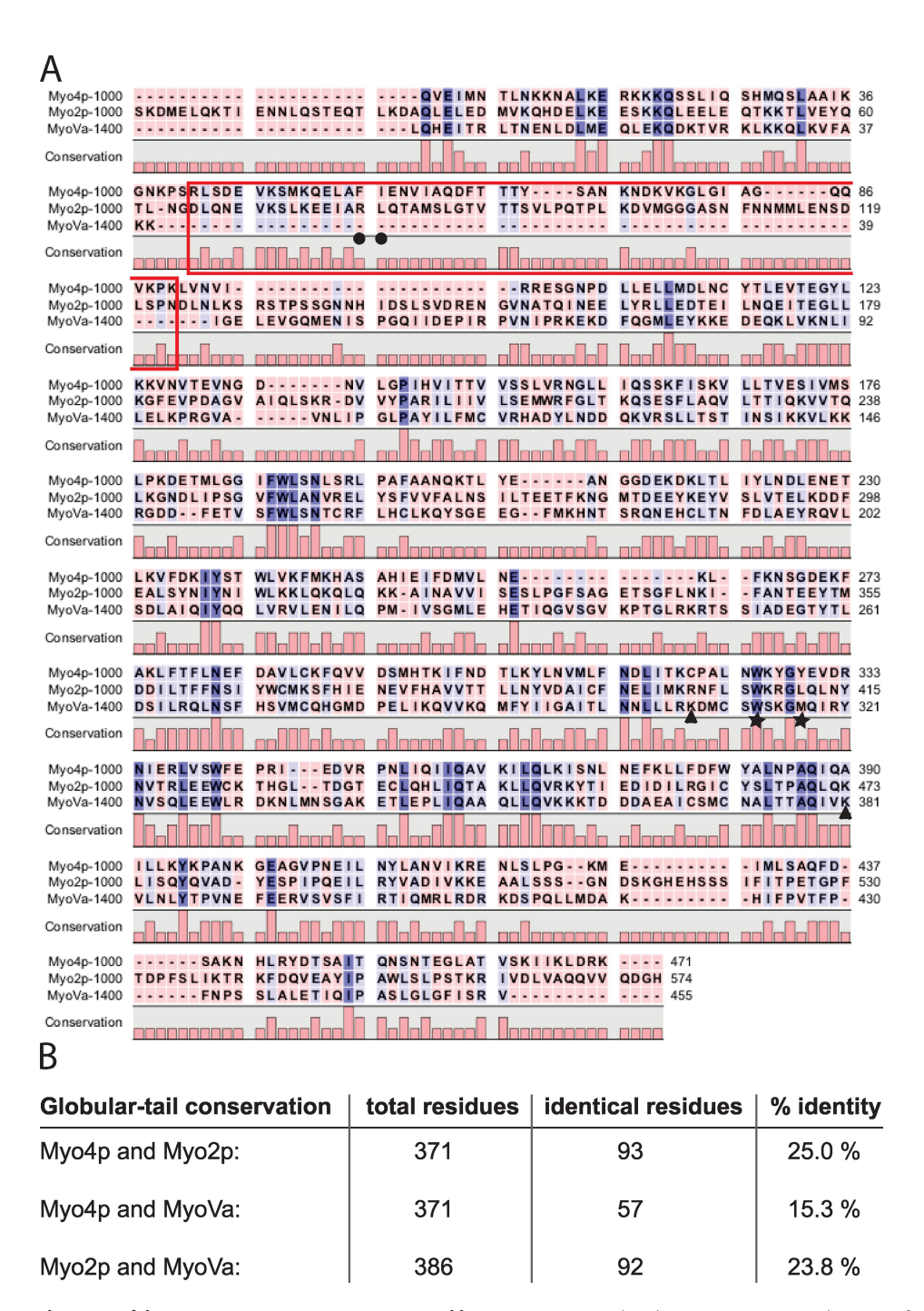


Figure S2. **Sequence alignment of the type V myosins Myo4p, Myo2p, and human MyoVa.** (A) The alignment starts at residue 1000 for both Myo4p and Myo2p and at residue 1400 for MyoVa. The color code indicates nonconserved residues in red and highly conserved residues in dark blue. The red box highlights the sequence alignment for the protease-sensitive linker region of Myo4p. Closed circles and asterisks mark pairs of residues in the linker region and the globular tail, respectively, which result in impaired She3p interaction and ASH1 mRNA localization upon mutation (Fig. 1, A and E and Fig. 6). Closed triangles indicate residues involved in the autoinhibition of type V myosins. They are conserved in Myo2p and MyoVa, but not in Myo4p (see also Fig. S4). Alignment was calculated with the program JPred and the graphic was generated with the program CLC-free-workbench (CLCbio). (B) Table comparing the number of residues identical in all three type V myosins that are exposed to the Myo4p-GT surface with the number of buried residues.

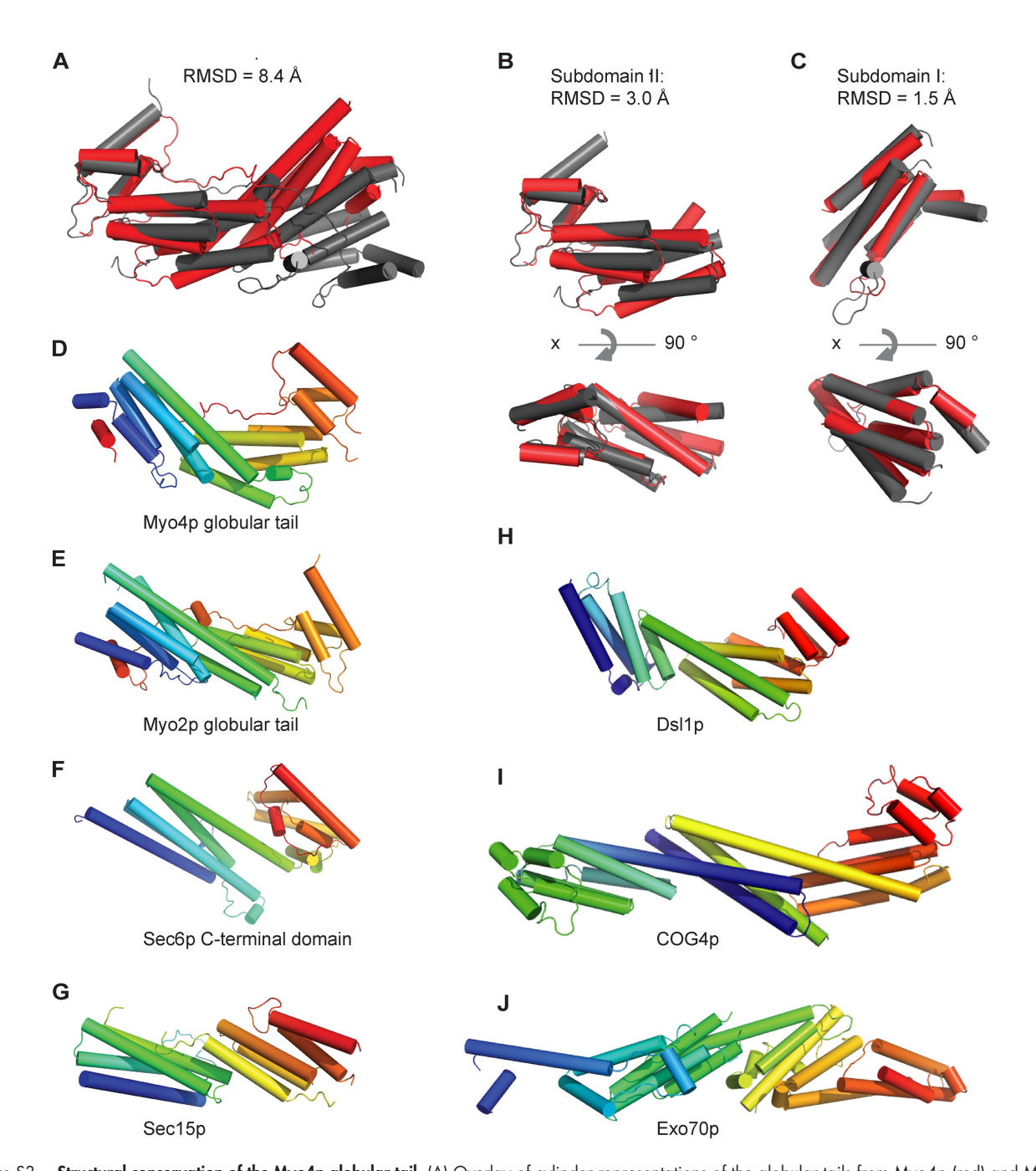


Figure S3. **Structural conservation of the Myo4p globular tail.** (A) Overlay of cylinder representations of the globular tails from Myo4p (red) and Myo2p (gray) yield a relatively large RMSD value of 8.4 Å. In contrast, the individual subdomains I and II (B and C) show a much higher degree of structural similarity. (D–I) A database search with the DALI algorithm and the Myo4p globular tail (D) as template yielded strong structural similarity to the C-terminal domain of Myo2p (E) (PDB code 2F6H; Pashkova et al., 2006), to the C-terminal domain of Sec6p (F) (PDB-ID: 2FII, chain 2, Z-score: 16.0; RMSD: 4.4 Å for 304 α-carbon pairs; Sivaram et al., 2006), to Sec15p (G) (PDB-ID: 2A2F, chain X, Z-score: 11.3; RMSD: 5.3 Å for 223 α-carbon pairs; Wu et al., 2005), to the C-terminal domain of Dsl1p (H) (PDB-ID: 3K8P, chain C, Z-score: 13.8; RMSD: 6.4 Å for 263 α-carbon pairs; Ren et al., 2009), to COG4 (I) (PDB-ID: 3HR0, chain A, Z-score: 11.1; RMSD: 3.9 for 209 α-carbon pairs; Richardson et al. 2009), and to Exo70p (I) (PDB-ID: 2B1E, chain A, Z-score: 9.2; RMSD: 10.8 Å for 245 α-carbon pairs; Dong et al., 2005). Helices are highlighted as cylinders and colored in rainbow representation with the N terminus in blue and C terminus in red. Images were generated with PyMOL (DeLano Scientific LLC).

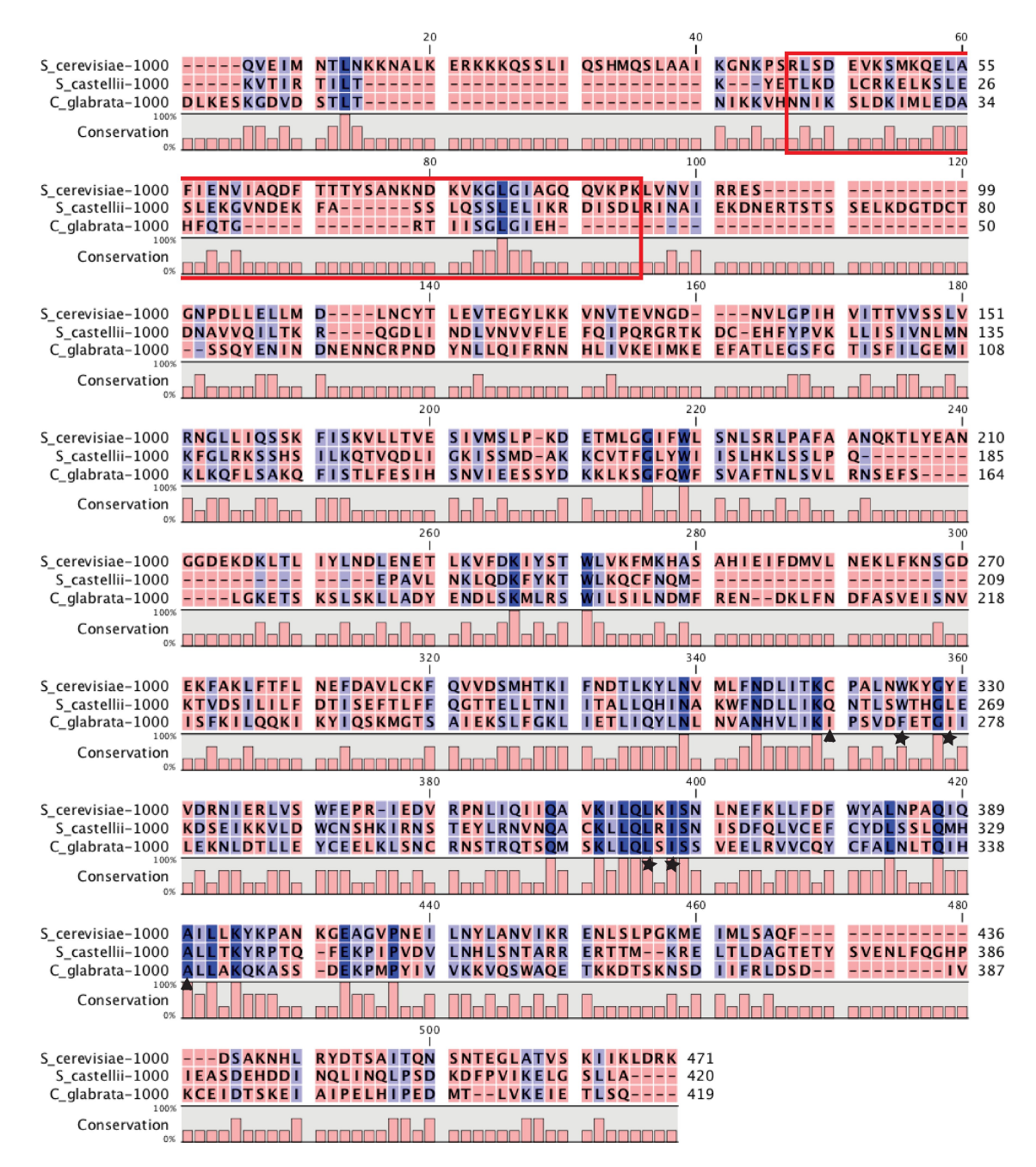
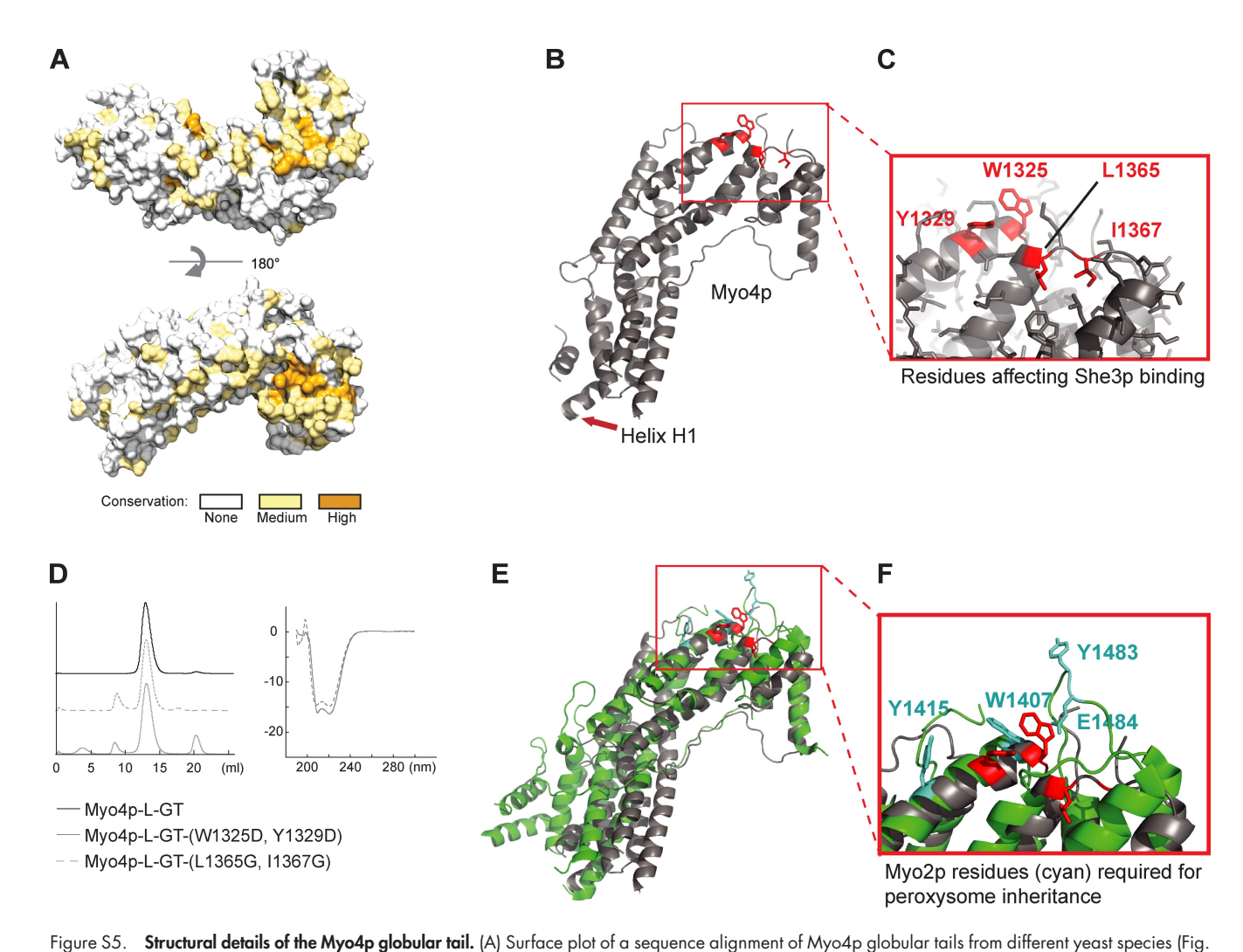


Figure S4. **Sequence alignment of Myo4p tails from different yeast species.** The alignment starts at residue 1000 for all Myo4p orthologues. The color code indicates nonconserved residues in red and highly conserved residues in dark blue. The red box highlights the sequence alignment for the protease-sensitive linker of Myo4p. Asterisks mark pairs of residues in the globular tail that result in impaired She3p interaction upon mutation (Fig. 6, A and B). Mutation of residues in position 1325 and 1329 was also shown to impair ASH1 mRNA localization (Fig. 6, A and C). Closed triangles indicate residues involved in the autoinhibition in other type V myosins, such as Myo2p and Myo5a (compare with Fig. S2 A). Myo4p orthologues lack the positively charged residues in this position, suggesting an absence of this inhibitory mechanism. The alignment was calculated with the program JPred and the graphic was generated with the program CLC-free-workbench (CLCbio).



S4). Dark yellow indicates residues identical in all three homologues, light yellow shows residues conserved in two homologues, and gray means no conserved in two homologues, and gray means no content in the property of the conserved in the property of the conserved in the property of the conserved in the homologues, and gray means no content in the property of the conserved region. The aromatic residues W1325 and Y1329 are located on top of helix H9, whereas residues L1365 and L1367 are located in a loop region between helices 10 and 11. (D) Size-exclusion chromatography (left) with a Superose 6 column shows that both mutant proteins have elution profiles indistinguishable from wild-type Myo4p globular tail. Circular dichroism spectroscopy further confirmed the α-helical nature of both mutants, as expected from the crystal structure. (E) Superposition of the Myo2p (green) and Myo4p (gray) globular tails. Residues shown on the Myo2p structure in cyan impair peroxisome inheritance upon mutation (Fagarasanu et al., 2009). For better comparison, Myo4p residues W1325, Y1329, L1365, and I1367 are highlighted in red. Orientation is identical to B. (F) Close-up of superposition from E. Orientation is identical to C.

References

- Bertrand, E., P. Chartrand, M. Schaefer, S.M. Shenoy, R.H. Singer, and R.M. Long. 1998. Localization of ASH1 mRNA particles in living yeast. *Mol. Cell.* 2:437–445. doi:10.1016/S1097-2765(00)80143-4
- Dong, G., A.H. Hutagalung, C. Fu, P. Novick, and K.M. Reinisch. 2005. The structures of exocyst subunit Exo70p and the Exo84p C-terminal domains reveal a common motif. Nat. Struct. Mol. Biol. 12:1094–1100. doi:10.1038/nsmb1017
- Fagarasanu, A., F.D. Mast, B. Knoblach, Y. Jin, M.J. Brunner, M.R. Logan, J.N. Glover, G.A. Eitzen, J.D. Aitchison, L.S. Weisman, and R.A. Rachubinski. 2009. Myosin-driven peroxisome partitioning in S. cerevisiae. J. Cell Biol. 186:541–554. doi:10.1083/jcb.200904050
- Pashkova, N., Y. Jin, S. Ramaswamy, and L.S. Weisman. 2006. Structural basis for myosin V discrimination between distinct cargoes. *EMBO J.* 25:693–700. doi:10.1038/sj.emboj.7600965
- Sivaram, M.V., M.L. Furgason, D.N. Brewer, and M. Munson. 2006. The structure of the exocyst subunit Sec6p defines a conserved architecture with diverse roles. *Nat. Struct. Mol. Biol.* 13:555–556. doi:10.1038/nsmb1096
- Ren, Y., C.K. Yip, A. Tripathi, D. Huie, P.D. Jeffrey, T. Walz, and F.M. Hughson. 2009. A structure-based mechanism for vesicle capture by the multisubunit tethering complex Dsl1. Cell. 139:1119–1129. doi:10.1016/j.cell.2009.11.002
- Richardson, B.C., R.D. Smith, D. Ungar, A. Nakamura, P.D. Jeffrey, V.V. Lupashin, and F.M. Hughson. 2009. Structural basis for a human glycosylation disorder caused by mutation of the COG4 gene. *Proc. Natl. Acad. Sci. USA*. 106:13329–13334. doi:10.1073/pnas.0901966106
- Wu, S., S.Q. Mehta, F. Pichaud, H.J. Bellen, and F.A. Quiocho. 2005. Sec15 interacts with Rab11 via a novel domain and affects Rab11 localization in vivo. *Nat. Struct. Mol. Biol.* 12:879–885. doi:10.1038/nsmb987